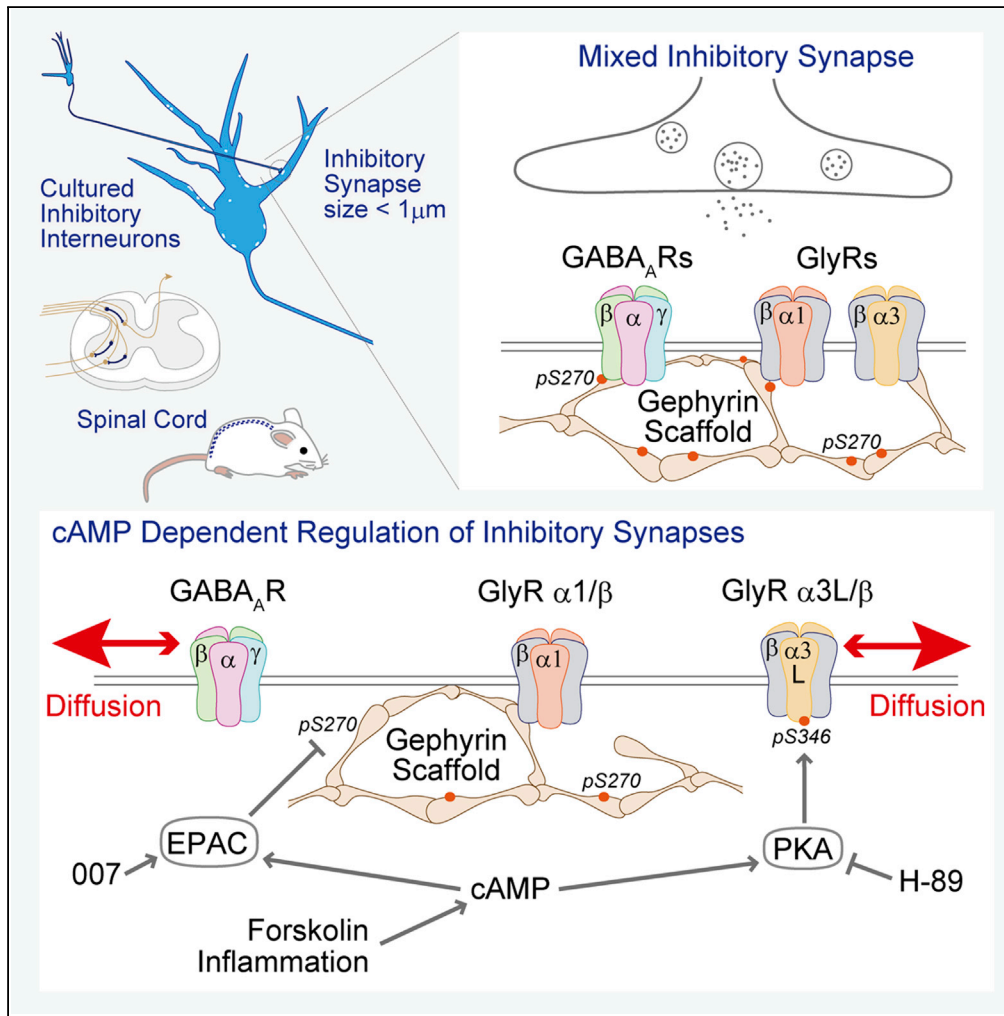**Article**

cAMP-EPAC-Dependent Regulation of Gephyrin Phosphorylation and GABA$_A$R Trapping at Inhibitory Synapses

Fumihiro Niwa,
Angela Patrizio,
Antoine Triller,
Christian G.
Specht

christian.specht@inserm.fr

HIGHLIGHTS

Differential signaling downstream of cAMP regulates mixed inhibitory synapses

EPAC reduces gephyrin S270 phosphorylation but not the copy numbers at synapses

Gephyrin de-phosphorylation reduces GABA$_A$R binding and increases receptor diffusion

PKA phosphorylation of GlyRα3L at residue S346 mobilizes synaptic receptors

Article

cAMP-EPAC-Dependent Regulation of Gephyrin Phosphorylation and GABA$_A$R Trapping at Inhibitory Synapses

Fumihiro Niwa,[1,2] Angela Patrizio,[1,2] Antoine Triller,[1] and Christian G. Specht[1,3,*]

SUMMARY

GABA$_A$ and glycine receptors are thought to compete for gephyrin-binding sites at mixed inhibitory synapses. Changes in the occupancy of one receptor type are therefore expected to have opposite effects on the clustering of the other receptors. This does not explain, however, whether different receptors can be regulated independently from one another. Here we show that cAMP-dependent signaling reduces gephyrin phosphorylation at residue S270 in spinal cord neurons. Although no ultrastructural changes of the synaptic scaffold were detected using super-resolution imaging, gephyrin de-phosphorylation was associated with a selective increase in GABA$_A$R diffusion and the loss of the receptors from synapses. As opposed to the PKA-dependent dispersal of α3-containing GlyRs, the regulation of gephyrin phosphorylation and GABA$_A$R dynamics acts via non-canonical EPAC signaling. Subtype-specific changes in receptor mobility can thus differentially contribute to changes in inhibitory synaptic strength, such as the disinhibition of spinal cord neurons during inflammatory processes.

INTRODUCTION

Inhibitory neurotransmission in the spinal cord is shaped by the balance between GABA$_A$ and glycine receptors that co-localize at the majority of synapses (Dumoulin et al., 2000; Geiman et al., 2002; Todd et al., 1996) and that are activated by the co-release of the two neurotransmitters from presynaptic vesicles (Aubrey and Supplisson, 2018; Jonas et al., 1998; Shrivastava et al., 2011). GABA$_A$Rs and GlyRs bind to the same region of the synaptic scaffold protein gephyrin (Kim et al., 2006; Kowalczyk et al., 2013; Maric et al., 2011; Tretter et al., 2011), which is thought to create strong competition between the receptors for synaptic binding sites. As a consequence, the main parameters controlling receptor trapping at mixed inhibitory synapses are the number of receptors, the number of available binding sites, and the relative affinity of the receptors for these sites (discussed in Specht, 2019). Plastic changes in the strength of receptor-gephyrin interactions are expected to shift the equilibrium between GABA$_A$Rs and GlyRs and alter the functional profile of mixed inhibitory synapses.

Post-translational modifications of gephyrin regulate the clustering of the scaffold protein and hence the number of receptor binding sites at synapses (Groeneweg et al., 2018). Phosphorylation of amino acid residue S270 of gephyrin appears to be particularly important for the clustering of gephyrin at GABAergic synapses, causing a variety of changes in the number, size, and intensity of synaptic clusters (Battaglia et al., 2018; Ghosh et al., 2016; Kalbouneh et al., 2014; Kuhse et al., 2012; Tyagarajan et al., 2011, 2013). The synaptic copy numbers of gephyrin and receptor complexes often change in synchrony owing to their reciprocal stabilization at synapses; however, it is unclear whether S270 phosphorylation acts on gephyrin oligomerization or on receptor-gephyrin binding (Specht, 2019). From a mechanistic point of view, gephyrin is known to assume various conformational states (Sander et al., 2013) that could mediate the downstream effects of S270 phosphorylation.

The intracellular domains (ICDs) of GABA$_A$Rs and GlyRs are subject to post-translational modifications that target the receptors' gephyrin-binding motifs (Mukherjee et al., 2011; Specht et al., 2011). It was recently shown that receptor-gephyrin interactions are also modulated by conformational changes associated with receptor activity (Gouzer et al., 2014; Patrizio et al., 2017). These studies suggest that in addition to the primary interaction domains, the strength of receptor-gephyrin binding is controlled by mechanisms that are related to the channel function. To test this idea, we set out to investigate whether the cyclic AMP (cAMP)-dependent reduction of glycinergic transmission during inflammation (Harvey et al., 2004) is accompanied by changes in receptor mobility. We found that phosphorylation of GlyRα3 at amino acid residue S346 by protein kinase A (PKA) indeed disrupted receptor trapping at spinal cord synapses.
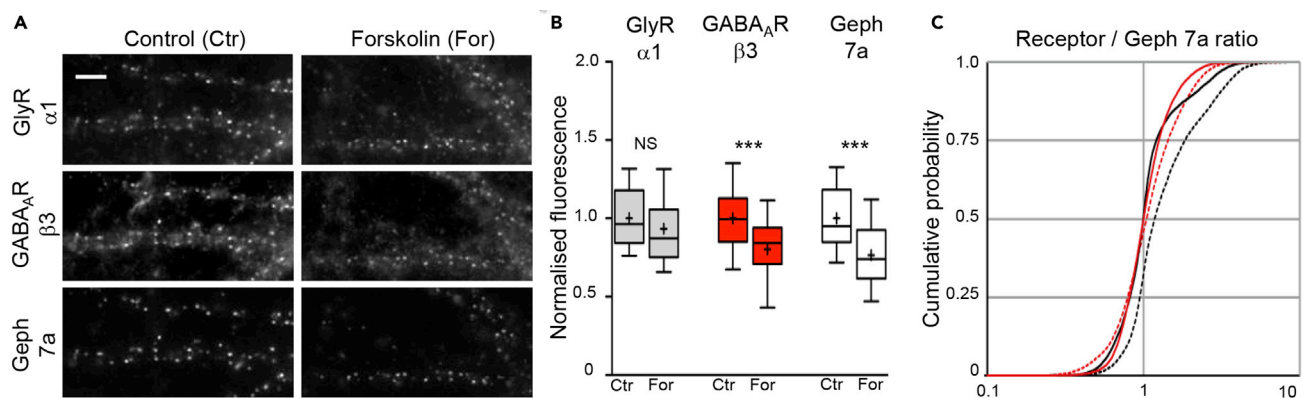
Figure 1. Forskolin Reduces GABA$_A$R and Gephyrin Immunoreactivity at Spinal Cord Synapses

(A) Triple immunolabeling of endogenous GlyRs, GABA$_A$Rs, and gephyrin in cultured rat spinal cord neurons (DIV16). Cells were treated with 20 μM forskolin (For) or kept under control conditions for 30 min (Ctr; vehicle 0.2% ethanol), fixed, and stained with antibodies against the GlyRα1 and GABA$_A$Rβ3 subunits, and with the rat gephyrin antibody mAb7a (Geph 7a, Synaptic Systems). Scale bar, 5 μm.

(B) Quantification of the integrated fluorescence intensity at synaptic GlyR puncta in the three channels (cell-by-cell analysis, arbitrary units normalized to the control condition in each channel; data are represented as 10%, 25%, 50% (median), 75%, and 90% percentiles; the mean is indicated as a cross; n_{Ctr} = 86, n_{For} = 79 cells from 6 coverslips and 3 independent experiments; ***p < 0.001, ANOVA).

(C) Cumulative probability of the ratio of the GlyR (black traces) or GABA$_A$R fluorescence intensities (red traces) relative to the Geph 7a immunoreactivity at synapses (control: solid lines, n_{Ctr} = 1.4 × 10^4; forskolin: dotted lines, n_{For} = 1.2 × 10^4 synapses).

Unexpectedly, we also identified a non-canonical cAMP signaling pathway that controls the phosphorylation status of gephyrin without affecting the size of gephyrin clusters and that leads to a specific reduction in GABA$_A$R clustering. These observations lend support to the concept that diverging signaling processes downstream of cAMP differentially regulate GABA$_A$R and GlyR numbers at mixed inhibitory synapses.

RESULTS

Reduction of GABA$_A$R Levels at Spinal Cord Synapses by Forskolin

To investigate the regulation of inhibitory synapses by cAMP-dependent mechanisms, we carried out immunocytochemical analysis of endogenous GlyRs, GABA$_A$Rs, and the scaffold protein gephyrin in two-week-old dissociated rat spinal cord neurons. cAMP-dependent signaling was induced with 20 μM forskolin for 30 min, followed by fixation of the neurons and triple labeling with specific antibodies against GlyRα1, GABA$_A$Rβ3, and gephyrin (Figure 1A). Quantification of the integrated fluorescence intensity of synaptic puncta did not reveal any significant differences of GlyR levels between control cultures treated with vehicle (0.2% ethanol, see Methods for details) and neurons exposed to forskolin (Figure 1B). We did, however, observe a strong reduction of both GABA$_A$R and gephyrin immunoreactivity in response to forskolin treatment. The effect of forskolin was similar in magnitude for GABA$_A$Rβ3 and gephyrin (p > 0.05, ANOVA), with a mean reduction to 80.2% ± 2.8% and 76.6% ± 3.0% (mean ± SEM, not background corrected) of the control value, respectively, suggesting that the two effects could be linked (Figure 1B).

Synapse-by-synapse analysis of the relative changes in receptor and gephyrin immunoreactivity confirmed that forskolin treatment had little effect on the GABA$_A$Rβ3/gephyrin ratio (Figure 1C, red traces). However, the apparent increase in the GlyRα1/gephyrin ratio in the presence of forskolin (black dotted line) was difficult to interpret, given that gephyrin levels directly control the number of receptor-binding sites (Specht et al., 2013). It appeared doubtful to us how GlyR levels could be maintained in the face of a 25% loss in the number of binding sites. One explanation could be that the internalized fraction of GlyRs is increased (Breitinger et al., 2018), without changing the total fluorescence intensity at synapses. We therefore carried out live surface labeling of GlyRα1 (Figure S1A). However, we did not observe any significant difference between the surface GlyRα1 levels in control conditions and after 30 min of 20 μM forskolin application (Figure S1B).

Forskolin Alters mAb7a Immunoreactivity but Not the Total Gephyrin at Synapses

The monoclonal gephyrin antibody mAb7a that was used in the above experiments is widely employed to quantify gephyrin levels at inhibitory synapses, despite the fact that it recognizes an epitope in the central domain of
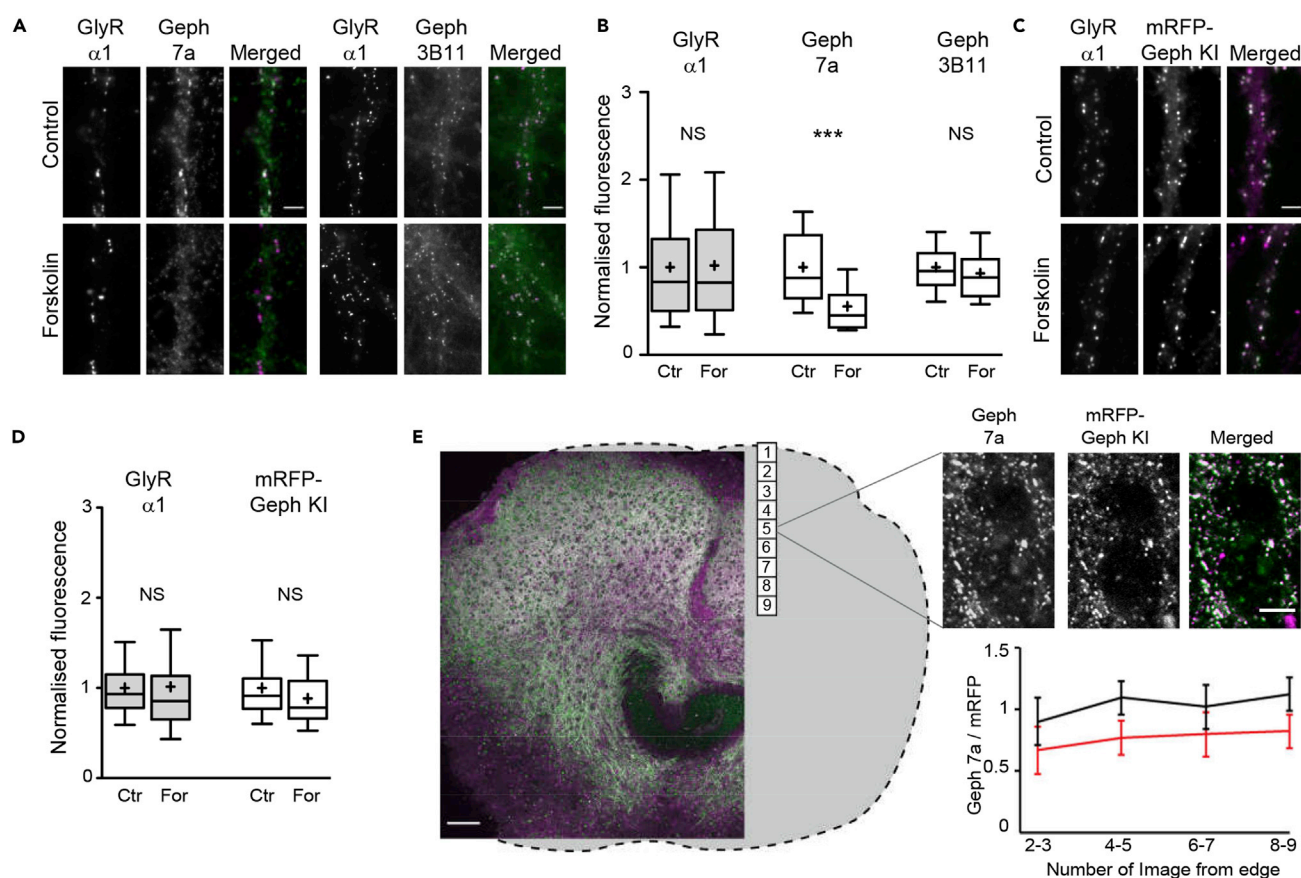
Figure 2. Gephyrin Protein Levels at Synapses Are Not Altered by Forskolin

(A) Sample images showing the effect of forskolin treatment on GlyRα1 (magenta in the merged image) and two different gephyrin antibodies (mAb7a and 3B11, green). Fluorescent signals from Geph 7a were reduced by forskolin, whereas GlyRα1 and Geph 3B11 were not affected. Scale bar, 5 μm.

(B) Integrated fluorescence intensity of endogenous gephyrin at rat spinal cord synapses was quantified in GlyRα1-positive puncta (background-corrected data). Geph 7a labeling was decreased by 45% ± 4% after 30-min treatment with 20 μM forskolin (For) compared with the control (***p < 0.001, ANOVA), whereas no significant changes (NS) were observed with Geph 3B11 (GlyRα1: n_{Ctr} = 149, n_{For} = 144 cells, 5 experiments; Geph 7a: n_{Ctr} = 60, n_{For} = 56, 2 experiments; Geph 3B11: n_{Ctr} = 89, n_{For} = 88 cells, 3 experiments). Data are represented as 10%, 25%, 50%, 75%, and 90% percentiles; the mean is indicated as a cross.

(C) Dissociated spinal cord cultures prepared from an mRFP-gephyrin knock-in mouse strain (mRFP-Geph KI, magenta) were treated with or without forskolin and then immunolabeled for GlyRα1 (green). Scale bar, 5 μm.

(D) No significant change in mRFP-Geph KI fluorescence and GlyRα1 immunoreactivity was observed (n_{Ctr} = 39; n_{For} = 40 cells, 1 experiment).

(E) Organotypic spinal cord cultures made from mRFP-gephyrin KI mice were treated at DIV21 with 20 μM forskolin for 60 min and fixed, labeled, and analyzed by confocal microscopy. Geph 7a immunoreactivity (green in merged image) and mRFP fluorescence (magenta) were quantified in a consecutive series of nine single-plane images taken from the dorsal edge of the slice toward the center (n_{Ctr} = 44, n_{For} = 57 images from 7–8 slices and 2 independent experiments; ***p < 0.0001 for the pooled data points for each condition, t test; data are shown as mean ± SD). The sample images represent a non-treated control slice; the gray outline illustrates the shape of the complete organotypic slice. Scale bar, 100 μm; zoomed images, 5 μm.

gephyrin that includes the phosphorylated serine residue S270 (Kuhse et al., 2012). To verify the observed reduction of gephyrin labeling after forskolin treatment we performed experiments with a different monoclonal antibody that binds to the gephyrin E-domain (3B11; Smolinsky et al., 2008). To our surprise, gephyrin immunoreactivity with the antibody 3B11 was not different in control and forskolin-treated neurons (p > 0.05, ANOVA, Figures 2A and 2B), whereas mAb7a labeling was strongly reduced (55.3% ± 4.2% of control, mean ± SEM, p < 0.001). Note that the data were corrected for the background, which explains the stronger reduction than in the previous experiment (Figure 1B, see methods for data analysis). Endogenous GlyRα1 labeling was not significantly different between the two conditions (p > 0.05), in agreement with our earlier data.

These observations raised our suspicion that the reduction in gephyrin labeling could be due to the mAb7a antibody and did not reflect any real change in the total gephyrin amount at synapses. We tested this
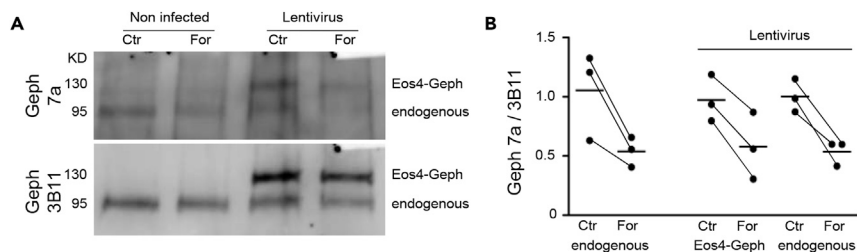
Figure 3. Forskolin Reduces Gephyrin Phosphorylation of Residue S270

(A) Western blotting of total protein fractions of rat spinal cord cultures exposed to forskolin (For) or kept in control condition (Ctr). Sequential labeling of the membranes with the gephyrin antibodies mAb7a and 3B11 identified the endogenous protein (95 kDa) and lentivirus-expressed mEos4b-gephyrin (130 kDa).

(B) For each Western blot membrane, we measured the intensity ratio of mAb7a/3B11 for all corresponding bands (endogenous gephyrin and recombinant mEos4b-gephyrin). Forskolin treatment reduced S270 phosphorylation of gephyrin by 45.8% as judged by the lower mAb7a/3B11 ratio (n = 9 bands per condition from 3 independent experiments, p < 0.001, paired t test).

hypothesis in spinal cord cultures derived from a knock-in mouse strain that expresses endogenous mRFP-tagged gephyrin (Machado et al., 2011). Neither GlyRα1 nor the total mRFP-gephyrin levels at synapses were altered by bath application of forskolin (Figures 2C and 2D; $p_{GlyRα1} > 0.05$, $p_{mRFP-Geph} > 0.05$, ANOVA), confirming that the treatment did not have a noticeable effect on the gephyrin molecule numbers at synapses.

To directly compare the effects of forskolin on mAb7a immunoreactivity and total mRFP-gephyrin levels in a more integrated system, we also conducted experiments in organotypic slice cultures from knock-in animals. Three-week-old spinal cord slice cultures were treated with 20 μM forskolin for 60 min, fixed, immunolabeled, and analyzed with confocal microscopy (Figure 2E). The mAb7a and mRFP-gephyrin fluorescence at synapses was quantified in single image planes that were taken from the dorsal edge of the slice toward the central region. We observed that the ratio of mAb7a/mRFP-gephyrin was reduced after forskolin treatment across all regions, demonstrating that mAb7a immunoreactivity is systematically reduced in different neuronal populations, and is not representative of the total synaptic gephyrin levels in our experimental paradigm.

Forskolin Reduces Gephyrin Phosphorylation of Residue S270

On the molecular level, the reduction in mAb7a immunoreactivity could be due either to the de-phosphorylation of gephyrin at residue S270 and/or to conformational changes induced by forskolin that render the epitope inaccessible for the antibody. To distinguish between these possibilities, we analyzed the gephyrin phosphorylation status by Western blotting (Figure 3). Dissociated rat spinal cord cultures were kept in medium containing 20 μM forskolin for 30 min, total protein fractions were collected in the presence of phosphatase inhibitors, and samples were separated by SDS-PAGE. Western blot membranes were sequentially probed with mAb7a antibody and with 3B11 that served as a loading control for total gephyrin (Figure 3A, first two lanes). Quantification of the mAb7a/3B11 ratio showed that forskolin treatment reduces mAb7a immunoreactivity by about 50% compared with the control condition (Figure 3B). It should be noted, however, that the mAb7a antibody is not well suited for Western blotting and produces only weak chemiluminescence signals.

To confirm the identity of the detected 95-kDa bands, we repeated the same experiment using cultures that had been infected with lentivirus driving the expression of mEos4b-gephyrin. The detection of an additional band at 130 kDa in these samples demonstrates the specificity of the mAb7a antibody (Figure 3A, lanes 3 and 4). What is more, the signals of both bands were weaker in the forskolin-treated sample, showing that the phosphorylation of both endogenous gephyrin and recombinant mEos4b-gephyrin are reduced by forskolin (Figure 3B). Across both pairs of samples and three independent experiments, the reduction in mAb7a/3B11 ratio was highly significant (mean reduction 45.8%, p < 0.001, paired t test, n = 9 bands per condition). These data indicate that forskolin treatment reduces S270 phosphorylation, although they do not exclude the fact that gephyrin could undergo concomitant conformational changes (Sander et al., 2013).
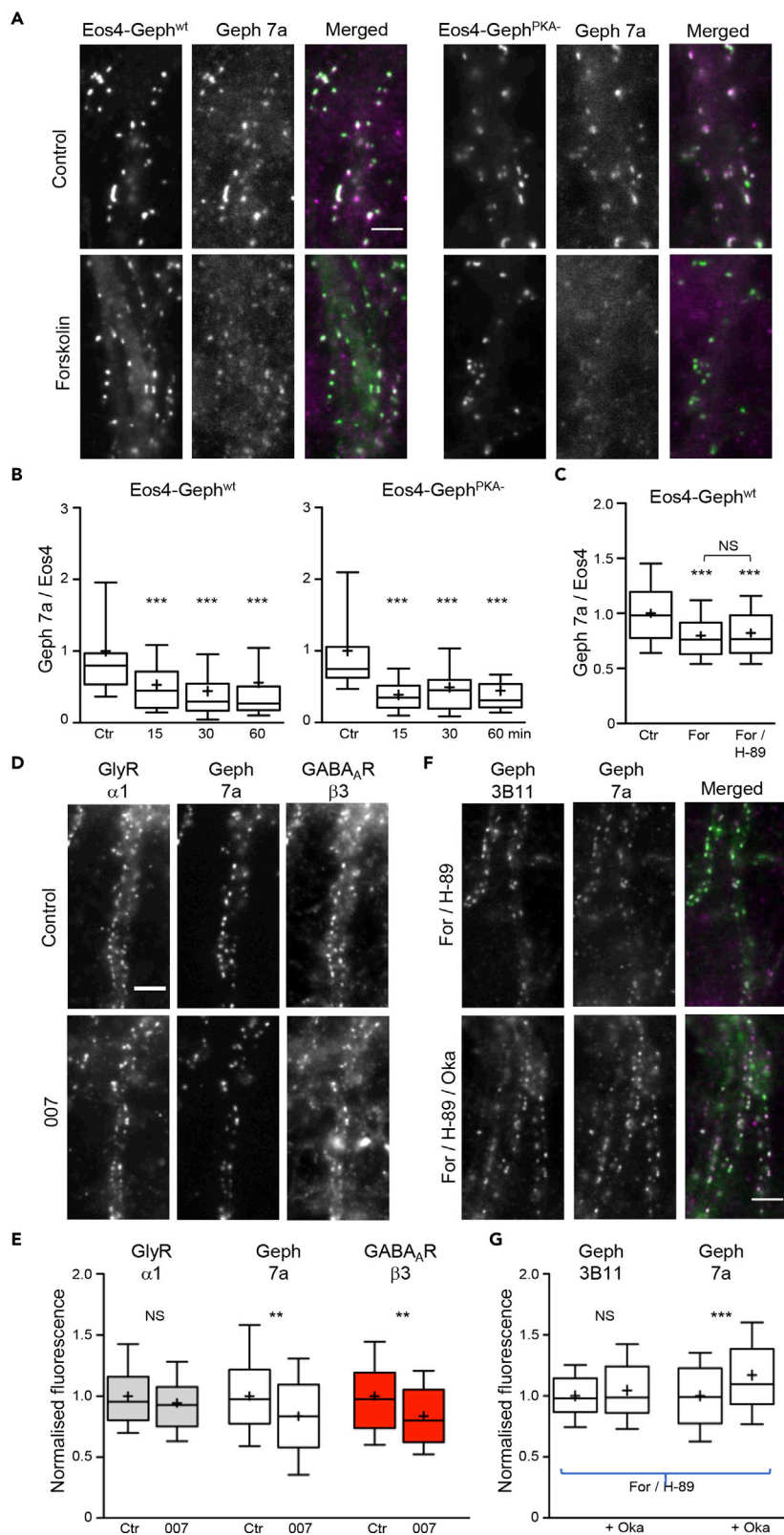
Figure 4. PKA-Independent Effect of Forskolin on Gephyrin Phosphorylation

(A) mEos4b-tagged wild-type (wt) and PKA-insensitive (PKA-) gephyrin were expressed in rat spinal cord neurons using lentiviral infection (green in merged image). Cells treated without (Ctr) or with forskolin (For) were labeled with Geph 7a antibody (magenta) and GlyRα1 antibody (shown in Figures S1D and S1E). Scale bar, 5 μm.

(B) Time course of the ratio of Geph 7a/Eos4-Geph fluorescence intensity (normalized for each construct to the control condition in each experiment) after forskolin application of up to 60 min (n > 40 cells for each construct and time point from 2 experiments, ***p < 0.001 against control, KW test).

(C) After 30-min exposure to forskolin, the Geph 7a/Eos4-Geph ratio was consistently reduced, regardless of the presence of the PKA inhibitor H-89 (n = 60 cells per condition, 2 experiments, ***p < 0.001 against control, ANOVA).

(D) Triple immunostaining of GlyRα1, Geph 7a, and GABA$_A$Rβ3 with or without the EPAC agonist 007 for 30 min. Scale bar, 5 μm.

(E) Normalized fluorescence intensity of 007-treated neurons (n_{Ctr} = 90, n_{007} = 83 cells from 3 experiments). EPAC activity significantly reduced Geph 7a and GABA$_A$Rβ3 labeling, but not GlyRα1 (**p < 0.01, ANOVA).

(F and G) Spinal cord neurons were treated for 30 min with forskolin and H-89 in the presence or absence of 40 nM okadaic acid (Oka). Blockade of phosphatase PP1/PP2A increased the Geph 7a signal (magenta), but not Geph 3B11 (green), at the synapses ($n_{For/H89}$ = 86 and $n_{For/H89+Oka}$ = 84 cells from 3 experiments, ***p < 0.001, t test). Scale bar, 5 μm. Data are represented as 10%, 25%, 50%, 75%, and 90% percentiles; the mean is indicated as a cross.

PKA-Independent Effect of Forskolin on Gephyrin Phosphorylation

PKA is considered as the main effector downstream of cAMP signaling. To characterize the mechanism by which forskolin leads to the de-phosphorylation of residue S270 of gephyrin, we tested the involvement of known *in vivo* PKA phosphorylation sites of gephyrin. Wild-type mEos4b-gephyrin and a PKA-phosphorylation-deficient variant carrying the amino acid substitutions S294A/S295A/S303A/S305A/S319A (Eos4-Geph^{PKA-}) were expressed in spinal cord neurons by lentivirus infection (Figures 4A and S1C), and synaptic gephyrin levels were quantified after treatment of the neurons with forskolin for different durations (15, 30, 60 min).

Immunolabeling with mAb7a antibody confirmed that S270 phosphorylation was decreased relative to the total Eos4-Geph^{wt} levels at synapses (mAb7a/Eos4 ratio, p < 0.001 at all time points versus control, Kruskal-Wallis (KW) test; Figure 4B, see also Figures S1D and S1E). Surprisingly, Eos4-Geph^{PKA-}-expressing neurons showed the same temporal profile, suggesting that forskolin did not act directly via any of the mutated PKA phosphorylation sites. We also applied forskolin together with the PKA inhibitor H-89 (Figure 4C). The mAb7a labeling was reduced to a similar level as in Eos4-Geph^{wt}-expressing neurons treated with forskolin without H-89 (p > 0.05, ANOVA). Therefore the effect of forskolin on gephyrin phosphorylation did not appear to be mediated by PKA.

We then considered the involvement of other cAMP-dependent signaling proteins, namely, the exchange proteins directly activated by cAMP (EPAC). Immunolabeling of EPAC shows a punctate distribution in spinal cord neurons that partially overlaps with gephyrin clusters (Figures S2A and S2B). Co-expression of N- and C-terminally tagged EPAC2 together with mRFP-gephyrin substantiated the presence of EPAC at inhibitory synapses (Figure S2C). The EPAC-specific agonist 007-AM led to a reduction of mAb7a labeling of endogenous gephyrin and of β3-containing GABA$_A$Rs (p < 0.01, ANOVA), but did not have any effect on GlyRα1 levels (Figures 4D and 4E). These effects were very similar to what had been observed with forskolin (Figure 1B). Together, the results indicate that EPAC and not PKA is responsible for the changes in gephyrin phosphorylation.

As EPAC has been reported to form a complex and act in concert with protein phosphatase PP2a (Hong et al., 2008), we treated cells for 15 min with or without 40 nM okadaic acid, an inhibitor of PP1/PP2a, and then added forskolin together with H-89 for further 30 min (Figures 4F and 4G). Okadaic acid reversed the forskolin effect, resulting in a significant increase in mAb7a, but not 3B11, labeling (p_{mAb7a} < 0.001, p_{3B11} = 0.20, t test). This is in agreement with an earlier study that has implicated PP1/PP2a in the de-phosphorylation of gephyrin at position S270 (Kalbouneh et al., 2014).

Single Molecule Localization Microscopy of Synaptic Gephyrin Clusters

To explore the downstream consequences of S270 de-phosphorylation on the organization of the gephyrin scaffold at inhibitory synapses, we did super-resolution single-molecule localization microscopy (SMLM) imaging of recombinant gephyrin tagged with the photoconvertible protein mEos4b in fixed spinal cord neurons (Figure 5A). Owing to the high spatial resolution of the technique, differences in the ultrastructure of the synapse and in the distribution of scaffold proteins can be identified on the nanometer scale. As
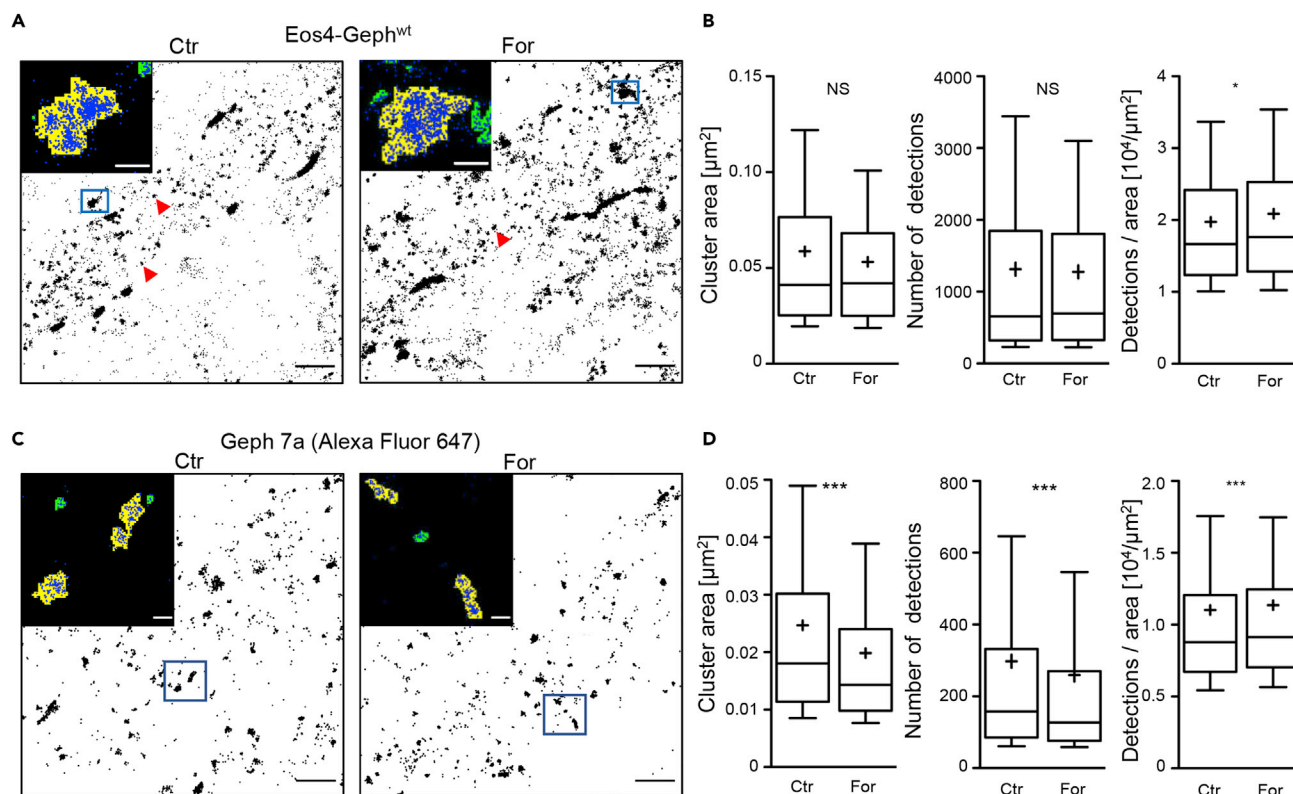
Figure 5. SMLM Super-resolution Imaging of Synaptic Gephyrin Clusters

(A) Single molecule detections (shown as black dots, or blue in the zoomed images) of recombinant mEos4b-gephyrin expressed in spinal cord neurons in control condition (Ctr) or after forskolin application (For). Arrowheads indicate the positions of small, non-synaptic clusters arising from the repetitive detection of single mEos4b fluorophores. Dense synaptic clusters were identified based on cluster size and detection number in the pointillist images (yellow areas in the zoomed images, see Methods). Clusters with less than 200 detections were not considered (green areas). Scale bar, 1 μm; insert, 100 nm.

(B) Quantification of synaptic cluster areas, detection numbers, and detection densities (n_{Ctr} = 1,237, n_{For} = 894 clusters from 32 cells per condition and 3 independent experiments, *p < 0.05, MW test).

(C) dSTORM imaging of endogenous gephyrin labeled with mAb7a and secondary Alexa Fluor 647-coupled antibodies. Cluster analysis was done as in (A), with a lower threshold of 50 detections per cluster. Scale bar, 1 μm; insert, 100 nm.

(D) Quantification of the cluster area and the number of Alexa 647 detections shows a correlated decrease in the forskolin-treated neurons compared with control cells (n_{Ctr} = 8,162 clusters in 69 cells, n_{For} = 7,010 clusters in 68 cells, 3 experiments, ***p < 0.001, MW test). Data are shown as 10%, 25%, 50%, 75%, and 90% percentiles and the mean (cross).

judged from pointillist images of the single fluorophore detections, Eos4-Geph^{wt} is densely packed in synaptic clusters along the dendrites and on the somata of infected neurons. These clusters can be easily distinguished by their size and the number of detections from non-synaptic gephyrin molecules that are diffusely distributed throughout the cell (Figure 5A, arrowheads).

The quantification of gephyrin cluster sizes did not reveal any differences between control and forskolin-treated neurons (synapse-by-synapse analysis, median area$_{Ctr}$: 0.041 μm², area$_{For}$: 0.042 μm², p = 0.20, Mann-Whitney U-test [MW] test). Similarly, the number of mEos4b detections per cluster was not altered (Figure 5B). These data show that forskolin treatment did not affect the clustering of gephyrin molecules at synapses. The fact that the number of detections was the same in both experimental conditions was expected, because the mEos4b detections reflect the total gephyrin content of the synapse. Due to the large sample size (n > 800 synapses per condition), there was a significant difference in the detection density (Figure 5B, right panel). However, cell-by-cell analysis of the same data did not reveal any obvious difference of the absolute detection densities (Figure S3A).

Experiments were also carried out using dSTORM to identify changes in the distribution of phosphorylated pS270-gephyrin (Figure 5C). Here, endogenous gephyrin in fixed spinal cord neurons was labeled with
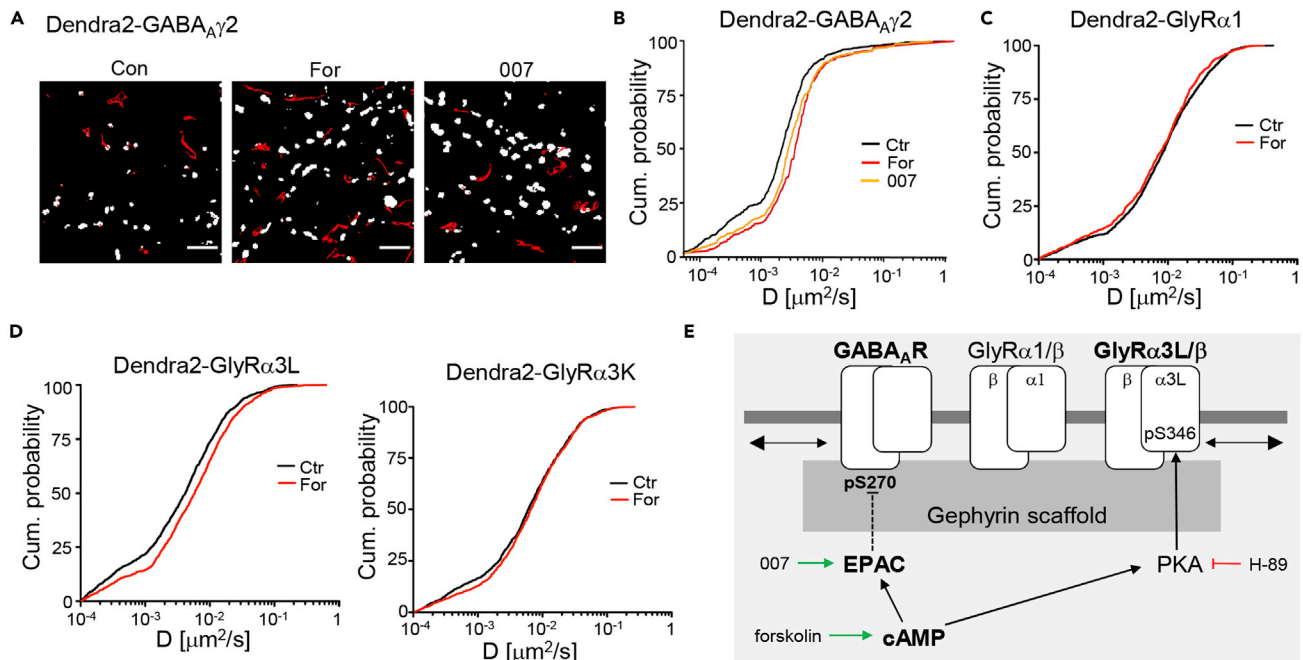
Figure 6. cAMP-Dependent Regulation of GABA$_A$R and GlyR Diffusion

(A) Quantum dot (QD) trajectories of Dendra2-GABA$_A$Rγ2-containing receptor complexes (red traces) in control neurons and in the presence of either forskolin or 007-AM. Synapses were identified with FM4-64 labeling (white areas). Scale bar, 5 μm.

(B) Cumulative probabilities of QD-tagged Dendra2-GABA$_A$Rγ2 diffusion coefficients at synapses in the three experimental conditions (median D values: D_{Ctr} = 0.0022 μm^2/s, D_{For} = 0.0031, D_{007} = 0.0028, n_{Ctr} = 730 trajectories from 41 cells, n_{For} = 318 trajectories from 42 cells, n_{007} = 384 trajectories from 40 cells, 7 coverslips per condition, 3 experiments).

(C) The median diffusion coefficients of Dendra2-GlyRα1 at spinal cord synapses were similar in the control and forskolin condition (in the absence of the drug, after a 30-min forskolin incubation; D_{Ctr} = 0.0083 μm^2/s, D_{For} = 0.0076, n > 1,000 trajectories from 5 experiments).

(D) Synaptic diffusion coefficients of Dendra2-GlyRα3L and α3K splice variants. Forskolin application specifically increased the speed of diffusion of Dendra2-GlyRα3L at synapses (α3L: D_{Ctr} = 0.0041, D_{For} = 0.0058, n > 1,000; α3K: D_{Ctr} = 0.0060 μm^2/s, D_{For} = 0.0066, n > 900 QD trajectories; 5 experiments).

(E) Model of cAMP-dependent pathways regulating inhibitory receptor dynamics at mixed spinal cord synapses, including the pharmacological agents used in this study (see text for details).

mAb7a and Alexa Fluor 647-coupled secondary antibodies. Pointillist images of Alexa 647 detections were analyzed in the same way as the mEos4b images, but with an adjusted threshold for cluster detection (see Methods). Both cluster size and detection numbers showed a significant reduction after forskolin treatment (median area$_{control}$: 0.018 μm^2, area$_{forskolin}$: 0.014 μm^2, p < 0.001, MW test, see Table S2). Interestingly, the detection density of pS270-gephyrin clusters was not noticeably changed by forskolin (Figures 5D and S3B). Our interpretation of these data is that the de-phosphorylation of gephyrin occurs within specific sub-synaptic domains, but that it has no influence on the overall organization of the gephyrin scaffold.

cAMP-Dependent Regulation of GABA$_A$R Diffusion

As the S270 phosphorylation status did not appear to have any effect on gephyrin clustering as such, we explored possible consequences of S270 de-phosphorylation on receptor binding at synapses. Single particle tracking with quantum dots was carried out in infected rat spinal cord neurons expressing different Dendra2-tagged receptor subunits. Diffusion coefficients were calculated from receptor trajectories at synapses as well as in the extrasynaptic plasma membrane (Figure 6A).

In the presence of forskolin, the diffusion of Dendra2-GABA$_A$Rγ2 receptors at synapses was considerably faster compared with control neurons (Figure 6B; p < 0.001, KW test). The same was true for neurons treated with the EPAC agonist 007-AM (p < 0.001). In contrast, we did not observe any changes in the diffusion of GlyRα1-containing receptors following a 30-min exposure to forskolin (Figure 6C). These data indicate that cAMP-dependent signaling via EPAC acts specifically on GABA$_A$R-gephyrin binding, which is reflected in an increased mobility of the receptor at synapses.

Neurons in the dorsal horn of the spinal cord relay nociceptive signals from primary sensory neurons to the brain. The release of prostaglandin E_2 (PGE_2) during inflammation leads to the central disinhibition of the nociceptive pathways by blocking GlyRα3-containing receptor complexes in a PKA-dependent manner (Harvey et al., 2004). Given the known regulation of GlyRα3 by PKA in the context of inflammatory pain, we therefore looked at receptor diffusion in neurons expressing the splice variants Dendra2-GlyRα3L and α3K. The variant GlyRα3L contains a 15-amino acid insertion in the proximity of the PKA phosphorylation site S346 (Harvey et al., 2004; Nikolic et al., 1998). The mobility of GlyRα3K-containing receptors was not changed, whereas the GlyRα3L variant was accelerated significantly after forskolin application (p < 0.001, KW test; Figure 6D), suggesting that forskolin weakened the gephyrin binding of GlyRα3L-containing receptor complexes. This fits with immunocytochemical data that showed a reduction of Dendra2-GlyRα3L levels at synapses in response to forskolin (Figure S4). Moreover, mutagenesis of GlyRα3L at position S346 abolished the PKA-dependent reduction of synaptic receptor levels (Figure S5). In conclusion, separate cAMP pathways act on GABA_ARs and GlyRα3L/β complexes at mixed inhibitory synapses through post-translational modifications targeting gephyrin as well as individual receptor subtypes (Figure 6E).

DISCUSSION

The main result of this study is that cAMP-dependent EPAC signaling reduces gephyrin phosphorylation at the amino acid residue S270, weakening the GABA_AR-gephyrin interaction and leading to the selective dispersal of GABA_ARs from mixed inhibitory synapses in spinal cord neurons.

Gephyrin Clustering and the Role of S270 Phosphorylation

Labeling of gephyrin with the widely used antibody mAb7a showed that immunoreactivity of synaptic gephyrin clusters was substantially reduced in response to forskolin. As the antibody is specific for an epitope that includes the phosphorylated residue S270 of gephyrin (Kuhse et al., 2012), these data indicated that forskolin treatment causes a marked change in the phosphorylation status of endogenous and recombinant gephyrin in cultured spinal cord neurons as well as in organotypic slices.

The phosphorylation of gephyrin at residue S270 has been implicated in the regulation of gephyrin clustering at GABAergic synapses (Groeneweg et al., 2018). Several studies suggested that the phosphorylation-deficient gephyrin variant S270A gives rise to a higher number (Tyagarajan et al., 2011, 2013) or greater intensity and size of synaptic gephyrin clusters (Battaglia et al., 2018). We did not observe any significant changes in the total synaptic gephyrin levels, suggesting that S270 phosphorylation does not affect gephyrin clustering as such. This is consistent with the data of Kuhse and colleagues, who did not see any obvious changes of gephyrin clustering by S270 de-phosphorylation following the inhibition of Cdk5 (Kalbouneh et al., 2014; Kuhse et al., 2012).

Moreover, we did not detect any ultrastructural changes of the synaptic gephyrin scaffold using SMLM of mEos4b-tagged gephyrin in spinal cord cultures treated with forskolin. Endogenous pS270-gephyrin occupied a smaller synaptic area than total Eos4-Geph^wt as judged by dSTORM imaging. Upon forskolin treatment, the pS270 area was further reduced, whereas the detection density remained unchanged. These data are at odds with the observed differences in the density of phosphorylation variants of gephyrin that were overexpressed in primary hippocampal neurons (Battaglia et al., 2018). Even though the overall clustering of gephyrin was not dependent on its phosphorylation, our super-resolution images suggest that the pS270 form is concentrated in specialized sub-synaptic domains (Pennacchietti et al., 2017). However, it cannot be ruled out that these results are influenced by the stochasticity of dSTORM imaging (Yang and Specht, 2020).

A possible explanation for the conflicting findings is that gephyrin residue S270 is the target of converging signaling pathways, which means that its phosphorylation could involve additional, as yet unidentified post-translational modifications. After all, gephyrin contains more than 50 known *in vivo* modifications (see PhosphoSitePlus database, www.phosphosite.org; Hornbeck et al., 2015). For example, the phosphorylation of S268 by ERK1/2 (Tyagarajan et al., 2013), SUMOylation, or acetylation of gephyrin (Ghosh et al., 2016) could shape the responses downstream of S270 phosphorylation. In our experiments, the silencing of multiple putative PKA sites of gephyrin (including residues S303 and S305; Flores et al., 2015) did not induce any changes in cluster intensity ($I_{Geph\ PKA-} = 1.001 \pm 0.087$ of the wild-type construct, mean ± SEM, n = 42 cells, 2 experiments), ruling out that the phosphorylation of these sites by PKA could have counteracted an effect of pS270 on gephyrin clustering.

We therefore conclude that S270 phosphorylation does not regulate gephyrin clustering, that is to say that it has no effect on gephyrin-gephyrin binding. Instead, our data point to a model whereby S270 phosphorylation promotes the GABA$_A$R-gephyrin interaction (Figure 6E). This is in line with the loss of GABA$_A$R clustering in response to S270 de-phosphorylation after Cdk5 inhibition (Kalbouneh et al., 2014). The mobilization of GABA$_A$Rs does not have major structural consequences at mixed inhibitory synapses in the spinal cord, where GlyR-gephyrin interactions maintain the stability of the synaptic scaffold. In contrast, GABA$_A$R dispersal is followed by a rapid loss of gephyrin at purely GABAergic synapses owing to the reciprocal stabilization of receptors and scaffold proteins (e.g., Niwa et al., 2012). A higher fraction of pS270 may also explain how synaptic GABA$_A$R levels can be maintained during long-term application of diazepam, despite a substantial reduction in total gephyrin content (Lorenz-Guertin et al., 2019). In our view, this model can therefore reconcile some of the variable experimental results that have been reported.

Independence of GABA$_A$R and GlyR Binding at Mixed Inhibitory Synapses

The reduction of GABA$_A$R-gephyrin binding by pS270 de-phosphorylation is remarkable in that it regulates receptor diffusion in a subtype-specific manner by targeting the gephyrin scaffold itself. Post-translational modifications of the ICDs of GABA$_A$Rs and GlyRs have been shown to control the strength of individual receptor-gephyrin interactions (Mukherjee et al., 2011; Petrini et al., 2014; Specht et al., 2011). As the inhibitory receptors bind to overlapping sites of gephyrin (Maric et al., 2011; Tretter et al., 2011) they directly compete for synaptic binding sites. This is exemplified by the opposite changes of α2- versus α5-containing GABA$_A$R dynamics at hippocampal synapses (Gerrow and Triller, 2014), where the reduction in the affinity of one receptor type allows another receptor to occupy the liberated binding sites.

The fact that forskolin treatment specifically interfered with the clustering of GABA$_A$Rs (and GlyRα3) at synapses, but did not affect GlyRα1, shows that receptor levels can also be regulated separately, without prompting a compensatory effect (Figure 6E). Long-term blockade of network activity by tetrodotoxin likewise reduced GABA$_A$R levels independently of GlyRs (Specht et al., 2013). These observations imply that there is only a limited direct competition between receptors at mixed inhibitory synapses. Given the non-identity of the gephyrin-binding motifs (e.g., Grunewald et al., 2018; Kowalczyk et al., 2013; Maric et al., 2014), it is feasible that S270 de-phosphorylation and potentially associated conformational changes could only affect the binding of certain receptor subtypes. This raises the new concept that the synaptic gephyrin scaffold displays distinct, receptor-specific binding modes.

If different receptors can be regulated independently from one another, what then is the fate of the liberated binding sites? Although we cannot exclude that GABA$_A$Rs with a different subunit composition replace the β3-containing receptors, the most likely explanation is that the excessive binding sites are lost over time through the dissociation of gephyrin molecules from the synaptic cluster. This is consistent with the observation of a delayed reduction in mEos4b-gephyrin levels during long forskolin applications (Figures S1D and S1E). There was also a trend that GlyRs decline after prolonged exposure to forskolin, suggesting that S270 de-phosphorylation could possibly affect GlyR-gephyrin binding. In view of the high affinity of the GlyRβ-gephyrin interaction, however, these processes are expected to take place on a much longer timescale and to a lesser degree (Specht, 2019).

Another possibility for the relative independence of GABA$_A$R clustering is the implication of alternative binding mechanisms. GABA$_A$Rγ2-containing receptors, for instance, can be recruited by neuroligin-2 via Lhfpl4 binding (Davenport et al., 2017; Yamasaki et al., 2017). The slight mismatch in the relative changes of GABA$_A$Rs and pS270 levels (Figure 1C, red traces) could indeed point to the existence of a gephyrin-independent mechanism. Yet the overall correspondence between GABA$_A$R and S270 phosphorylation levels suggests that GABA$_A$R clustering at mixed inhibitory synapses in spinal cord neurons relies predominantly on a gephyrin-related mechanism.

Integration of cAMP-Dependent Pathways Regulating Receptor Trapping at Synapses

The effect of forskolin on GABA$_A$R diffusion at synapses led us to assume initially that the mechanism would be dependent on protein kinase A. There is ample evidence that PKA-dependent phosphorylation regulates GABA$_A$R function and trafficking, often producing divergent effects (reviewed in Nakamura et al., 2015). Unexpectedly, we found that neither mutagenesis of PKA phosphorylation sites of gephyrin nor the PKA blocker H-89 inhibited pS270 de-phosphorylation and GABA$_A$R dispersal. It turned out that the GABA$_A$R loss was in fact caused by a different process, namely, the activation of EPAC (Robichaux and

Cheng, 2018). The presence of this cAMP-regulated guanine nucleotide exchange factor at inhibitory synapses (Figure S2) acting in parallel to PKA could have an important role in the regulation of inhibitory neurotransmission. In other words, cAMP could simultaneously trigger PKA and EPAC signaling processes, leading to complex downstream effects at inhibitory synapses.

For instance, PGE_2 is known to inhibit glycinergic currents in a PKA-dependent manner during inflammatory pain (Harvey et al., 2004). The GlyRα3 specificity of this effect comes from the presence of a PKA phosphorylation site at residue S346 in the ICD that is not present in GlyRα1. Phosphorylation of this site was shown to induce global conformational changes that extend to the agonist-binding pocket (Han et al., 2013). We found that forskolin treatment of Dendra2-GlyRα3L-expressing spinal cord neurons increased the mobility of the receptors, whereas no change was observed for GlyRα1. This suggests that changes in receptor-scaffold interaction parallel the changes in receptor activity (Harvey et al., 2004; Rajalu et al., 2009). In other words, the PKA-dependent inhibition of α3-containing GlyRs is associated with a weakening of the receptor-gephyrin interaction, lending further support to the hypothesis that the α-subunits of the GlyR can influence the strength of GlyRβ-gephyrin binding (Patrizio et al., 2017).

In addition, $GABA_AR\beta$ subunits contain conserved PKA sites in their ICDs, the phosphorylation of which regulates $GABA_AR$ function (McDonald et al., 1998), internalization (Kittler et al., 2005), and possibly gephyrin binding (Bohnsack et al., 2016; Kowalczyk et al., 2013). How these different signaling processes are integrated at mixed inhibitory synapses is not yet understood. Nonetheless, our data demonstrate that cAMP signaling has a significant impact on the trapping of $GABA_AR\gamma2$- and GlyRα3L-containing receptors (Figure 6E). Given that α1-containing GlyRs cannot compensate for this loss, a reduction of inhibitory neurotransmission seems inevitable. The dispersal of $GABA_ARs$ is likely to shift the inhibitory phenotype from a mixed to a purely glycinergic profile, with a fast, monophasic decay and lower charge transfer (Aubrey and Supplisson, 2018). This effect could exacerbate the disinhibition observed during pathological processes such as inflammatory pain. On a more positive note, the independence of $GABA_AR$ and GlyR regulation may also enable the development of specific pharmacological approaches that promote functional compensation.

Limitations of the Study

Different regulatory processes at inhibitory synapses may engage multiple and overlapping phosphorylation sites in the central domain of gephyrin. The phospho-specific antibody mAb7a therefore has to be seen as a sensitive tool that reports on one of these modifications that could be implicated in several regulatory mechanisms with different downstream consequences. This also raises concerns about the use of mAb7a antibody as a synaptic marker.

METHODS

All methods can be found in the accompanying Transparent Methods supplemental file.

DATA AND CODE AVAILABILITY

The raw data of this article are available from the corresponding author upon request.

SUPPLEMENTAL INFORMATION

Supplemental Information can be found online at https://doi.org/10.1016/j.isci.2019.11.013.

AUTHOR CONTRIBUTIONS

F.N., A.P., A.T., and C.G.S. planned the experiments; F.N., A.P., and C.G.S. performed the experiments and analyzed the data; F.N., A.P., and C.G.S. wrote the manuscript.

DECLARATION OF INTERESTS

The authors declare no competing interests.

REFERENCES

Aubrey, K.R., and Supplisson, S. (2018). Heterogeneous signaling at GABA and glycine co-releasing terminals. Front. Synaptic Neurosci. 10, 40.

Battaglia, S., Renner, M., Russeau, M., Come, E., Tyagarajan, S.K., and Levi, S. (2018). Activity-dependent inhibitory synapse scaling is determined by gephyrin phosphorylation and subsequent regulation of GABAA receptor diffusion. eNeuro 5, 1–20.

Bohnsack, J.P., Carlson, S.L., and Morrow, A.L. (2016). Differential regulation of synaptic and extrasynaptic alpha4 GABA(A) receptor populations by protein kinase A and protein kinase C in cultured cortical neurons. Neuropharmacology 105, 124–132.

Breitinger, U., Bahnassawy, L.M., Janzen, D., Roemer, V., Becker, C.M., Villmann, C., and Breitinger, H.G. (2018). PKA and PKC modulators affect ion channel function and internalization of recombinant alpha1 and alpha1-beta glycine receptors. Front. Mol. Neurosci. 11, 154.

Davenport, E.C., Pendolino, V., Kontou, G., McGee, T.P., Sheehan, D.F., Lopez-Domenech, G., Farrant, M., and Kittler, J.T. (2017). An essential role for the tetraspanin LHFPL4 in the cell-type-specific targeting and clustering of synaptic GABAA receptors. Cell Rep. 21, 70–83.

Dumoulin, A., Levi, S., Riveau, B., Gasnier, B., and Triller, A. (2000). Formation of mixed glycine and GABAergic synapses in cultured spinal cord neurons. Eur. J. Neurosci. 12, 3883–3892.

Flores, C.E., Nikonenko, I., Mendez, P., Fritschy, J.M., Tyagarajan, S.K., and Muller, D. (2015). Activity-dependent inhibitory synapse remodeling through gephyrin phosphorylation. Proc. Natl. Acad. Sci. U S A 112, E65–E72.

Geiman, E.J., Zheng, W., Fritschy, J.M., and Alvarez, F.J. (2002). Glycine and GABA(A) receptor subunits on Renshaw cells: relationship with presynaptic neurotransmitters and postsynaptic gephyrin clusters. J. Comp. Neurol. 444, 275–289.

Gerrow, K., and Triller, A. (2014). GABAA receptor subunit composition and competition at synapses are tuned by GABAB receptor activity. Mol. Cell Neurosci. 60, 97–107.

Ghosh, H., Auguadri, L., Battaglia, S., Simone Thirouin, Z., Zemoura, K., Messner, S., Acuna, M.A., Wildner, H., Yevenes, G.E., Dieter, A., et al.

(2016). Several posttranslational modifications act in concert to regulate gephyrin scaffolding and GABAergic transmission. Nat. Commun. 7, 13365.

Gouzer, G., Specht, C.G., Allain, L., Shinoe, T., and Triller, A. (2014). Benzodiazepine-dependent stabilization of GABA(A) receptors at synapses. Mol. Cell Neurosci. 63, 101–113.

Groeneweg, F.L., Trattnig, C., Kuhse, J., Nawrotzki, R.A., and Kirsch, J. (2018). Gephyrin: a key regulatory protein of inhibitory synapses and beyond. Histochem. Cell Biol. 150, 489–508.

Grunewald, N., Jan, A., Salvatico, C., Kress, V., Renner, M., Triller, A., Specht, C.G., and Schwarz, G. (2018). Sequences flanking the gephyrin-binding site of GlyRbeta tune receptor stabilization at synapses. eNeuro 5, 1–17.

Han, L., Talwar, S., Wang, Q., Shan, Q., and Lynch, J.W. (2013). Phosphorylation of alpha3 glycine receptors induces a conformational change in the glycine-binding site. ACS Chem. Neurosci. 4, 1361–1370.

Harvey, R.J., Depner, U.B., Wassle, H., Ahmadi, S., Heindl, C., Reinold, H., Smart, T.G., Harvey, K., Schutz, B., Abo-Salem, O.M., et al. (2004). GlyR alpha3: an essential target for spinal PGE2-mediated inflammatory pain sensitization. Science 304, 884–887.

Hong, K., Lou, L., Gupta, S., Ribeiro-Neto, F., and Altschuler, D.L. (2008). A novel Epac-Rap-PP2A signaling module controls cAMP-dependent Akt regulation. J. Biol. Chem. 283, 23129–23138.

Hornbeck, P.V., Zhang, B., Murray, B., Kornhauser, J.M., Latham, V., and Skrzypek, E. (2015). PhosphoSitePlus, 2014: mutations, PTMs and recalibrations. Nucleic Acids Res. 43, D512–D520.

Jonas, P., Bischofberger, J., and Sandkuhler, J. (1998). Corelease of two fast neurotransmitters at a central synapse. Science 281, 419–424.

Kalbouneh, H., Schlicksupp, A., Kirsch, J., and Kuhse, J. (2014). Cyclin-dependent kinase 5 is involved in the phosphorylation of gephyrin and clustering of GABAA receptors at inhibitory synapses of hippocampal neurons. PLoS One 9, e104256.

Kim, E.Y., Schrader, N., Smolinsky, B., Bedet, C., Vannier, C., Schwarz, G., and Schindelin, H. (2006). Deciphering the structural framework of

glycine receptor anchoring by gephyrin. Embo J. 25, 1385–1395.

Kittler, J.T., Chen, G., Honing, S., Bogdanov, Y., McAinsh, K., Arancibia-Carcamo, I.L., Jovanovic, J.N., Pangalos, M.N., Haucke, V., Yan, Z., et al. (2005). Phospho-dependent binding of the clathrin AP2 adaptor complex to GABAA receptors regulates the efficacy of inhibitory synaptic transmission. Proc. Natl. Acad. Sci. U S A 102, 14871–14876.

Kowalczyk, S., Winkelmann, A., Smolinsky, B., Forstera, B., Neundorf, I., Schwarz, G., and Meier, J.C. (2013). Direct binding of GABA(A) receptor beta2 and beta3 subunits to gephyrin. Eur. J. Neurosci. 37, 544–554.

Kuhse, J., Kalbouneh, H., Schlicksupp, A., Mukusch, S., Nawrotzki, R., and Kirsch, J. (2012). Phosphorylation of gephyrin in hippocampal neurons by cyclin-dependent protein kinase CDK5 at Ser-270 is dependent on collybistin. J. Biol. Chem. 287, 30952–30966.

Lorenz-Guertin, J.M., Bambino, M.J., Das, S., Weintraub, S.T., and Jacob, T.C. (2019). Diazepam accelerates GABAAR synaptic exchange and alters intracellular trafficking. Front. Cell Neurosci. 13, 163.

Machado, P., Rostaing, P., Guigonis, J.M., Renner, M., Dumoulin, A., Samson, M., Vannier, C., and Triller, A. (2011). Heat shock cognate protein 70 regulates gephyrin clustering. J. Neurosci. 31, 3–14.

Maric, H.M., Kasaragod, V.B., Hausrat, T.J., Kneussel, M., Tretter, V., Stromgaard, K., and Schindelin, H. (2014). Molecular basis of the alternative recruitment of GABA(A) versus glycine receptors through gephyrin. Nat. Commun. 5, 5767.

Maric, H.M., Mukherjee, J., Tretter, V., Moss, S.J., and Schindelin, H. (2011). Gephyrin-mediated gamma-aminobutyric acid type A and glycine receptor clustering relies on a common binding site. J. Biol. Chem. 286, 42105–42114.

McDonald, B.J., Amato, A., Connolly, C.N., Benke, D., Moss, S.J., and Smart, T.G. (1998). Adjacent phosphorylation sites on GABAA receptor beta subunits determine regulation by cAMP-dependent protein kinase. Nat. Neurosci. 1, 23–28.

Mukherjee, J., Kretschmannova, K., Gouzer, G., Maric, H.M., Ramsden, S., Tretter, V., Harvey, K.,

Davies, P.A., Triller, A., Schindelin, H., et al. (2011). The residence time of GABA(A)Rs at inhibitory synapses is determined by direct binding of the receptor alpha1 subunit to gephyrin. J. Neurosci. *31*, 14677–14687.

Nakamura, Y., Darnieder, L.M., Deeb, T.Z., and Moss, S.J. (2015). Regulation of GABAARs by phosphorylation. Adv. Pharmacol. *72*, 97–146.

Nikolic, Z., Laube, B., Weber, R.G., Lichter, P., Kioschis, P., Poustka, A., Mulhardt, C., and Becker, C.M. (1998). The human glycine receptor subunit alpha3. Glra3 gene structure, chromosomal localization, and functional characterization of alternative transcripts. J. Biol. Chem. *273*, 19708–19714.

Niwa, F., Bannai, H., Arizono, M., Fukatsu, K., Triller, A., and Mikoshiba, K. (2012). Gephyrin-independent GABA(A)R mobility and clustering during plasticity. PLoS One *7*, e36148.

Patrizio, A., Renner, M., Pizzarelli, R., Triller, A., and Specht, C.G. (2017). Alpha subunit-dependent glycine receptor clustering and regulation of synaptic receptor numbers. Sci. Rep. *7*, 10899.

Pennacchietti, F., Vascon, S., Nieus, T., Rosillo, C., Das, S., Tyagarajan, S.K., Diaspro, A., Del Bue, A., Petrini, E.M., Barberis, A., et al. (2017). Nanoscale molecular reorganization of the inhibitory postsynaptic density is a determinant of GABAergic synaptic potentiation. J. Neurosci. *37*, 1747–1756.

Petrini, E.M., Ravasenga, T., Hausrat, T.J., Iurilli, G., Olcese, U., Racine, V., Sibarita, J.B., Jacob, T.C., Moss, S.J., Benfenati, F., et al. (2014). Synaptic recruitment of gephyrin regulates surface GABAA receptor dynamics for the expression of inhibitory LTP. Nat. Commun. *5*, 3921.

Rajalu, M., Muller, U.C., Caley, A., Harvey, R.J., and Poisbeau, P. (2009). Plasticity of synaptic inhibition in mouse spinal cord lamina II neurons during early postnatal development and after inactivation of the glycine receptor alpha3 subunit gene. Eur. J. Neurosci. *30*, 2284–2292.

Robichaux, W.G., 3rd, and Cheng, X. (2018). Intracellular cAMP sensor EPAC: physiology, pathophysiology, and therapeutics development. Physiol. Rev. *98*, 919–1053.

Sander, B., Tria, G., Shkumatov, A.V., Kim, E.Y., Grossmann, J.G., Tessmer, I., Svergun, D.I., and Schindelin, H. (2013). Structural characterization of gephyrin by AFM and SAXS reveals a mixture of compact and extended states. Acta Crystallogr. D Biol. Crystallogr. *69*, 2050–2060.

Shrivastava, A.N., Triller, A., and Sieghart, W. (2011). GABA(A) receptors: post-synaptic co-localization and cross-talk with other receptors. Front. Cell Neurosci. *5*, 7.

Smolinsky, B., Eichler, S.A., Buchmeier, S., Meier, J.C., and Schwarz, G. (2008). Splice-specific functions of gephyrin in molybdenum cofactor biosynthesis. J. Biol. Chem. *283*, 17370–17379.

Specht, C.G. (2019). Fractional occupancy of synaptic binding sites and the molecular plasticity of inhibitory synapses. Neuropharmacology, 107493, https://doi.org/10.1016/j.neuropharm.2019.01.008.

Specht, C.G., Grunewald, N., Pascual, O., Rostgaard, N., Schwarz, G., and Triller, A. (2011). Regulation of glycine receptor diffusion properties and gephyrin interactions by protein kinase C. EMBO J. *30*, 3842–3853.

Specht, C.G., Izeddin, I., Rodriguez, P.C., El Beheiry, M., Rostaing, P., Darzacq, X., Dahan, M., and Triller, A. (2013). Quantitative nanoscopy of inhibitory synapses: counting gephyrin molecules and receptor binding sites. Neuron *79*, 308–321.

Todd, A.J., Watt, C., Spike, R.C., and Sieghart, W. (1996). Colocalization of GABA, glycine, and their receptors at synapses in the rat spinal cord. J. Neurosci. *16*, 974–982.

Tretter, V., Kerschner, B., Milenkovic, I., Ramsden, S.L., Ramerstorfer, J., Saiepour, L., Maric, H.M., Moss, S.J., Schindelin, H., Harvey, R.J., et al. (2011). Molecular basis of the gamma-aminobutyric acid A receptor alpha3 subunit interaction with the clustering protein gephyrin. J. Biol. Chem. *286*, 37702–37711.

Tyagarajan, S.K., Ghosh, H., Yevenes, G.E., Imanishi, S.Y., Zeilhofer, H.U., Gerrits, B., and Fritschy, J.M. (2013). Extracellular signal-regulated kinase and glycogen synthase kinase 3beta regulate gephyrin postsynaptic aggregation and GABAergic synaptic function in a calpain-dependent mechanism. J. Biol. Chem. *288*, 9634–9647.

Tyagarajan, S.K., Ghosh, H., Yevenes, G.E., Nikonenko, I., Ebeling, C., Schwerdel, C., Sidler, C., Zeilhofer, H.U., Gerrits, B., Muller, D., et al. (2011). Regulation of GABAergic synapse formation and plasticity by GSK3beta-dependent phosphorylation of gephyrin. Proc. Natl. Acad. Sci. U S A *108*, 379–384.

Yamasaki, T., Hoyos-Ramirez, E., Martenson, J.S., Morimoto-Tomita, M., and Tomita, S. (2017). GARLH family proteins stabilize GABAA receptors at synapses. Neuron *93*, 1138–1152.e6.

Yang, X., and Specht, C.G. (2020). Practical guidelines for two-color SMLM of synaptic proteins in cultured neurons. In Single Molecule Microscopy in Neurobiology, Y. Okada and N. Yamamoto, eds. (Springer).

Supplemental Information

cAMP-EPAC-Dependent Regulation

of Gephyrin Phosphorylation and GABA$_A$R

Trapping at Inhibitory Synapses

Fumihiro Niwa, Angela Patrizio, Antoine Triller, and Christian G. Specht

Transparent Methods

Expression constructs

The coding sequence (cds) of Dendra2 (Clontech 632546) was inserted 3' of the signal peptide (SP) into the full-length cds of mouse GABA$_A$Rγ2 (UniProt P22723-1, isoform 2L) in the lentivirus vector FUGW (Lois et al., 2002), to generate the replicon FU-Dendra2-GABA$_A$Rγ2. The lentivirus constructs FU-Dendra2-GlyRα1 and FU-Dendra2-GlyRα3L (long isoform) were described previously (Patrizio et al., 2017). A short isoform lacking the residues T[325]EAFALEKFYRFSDM[339] of the ICD of GlyRα3 (Nikolic et al., 1998) was also constructed (FU-Dendra2-GlyRα3K). The phosphorylation variants FU-mEos4b-GlyRα3L^{S346A} and FU-mEos4b-GlyRα3L^{S346D} were obtained by site-directed mutagenesis from the mEos4b-version of the wild-type GlyRα3L construct (FU-mEos4b-GlyRα3L). Plasmid FU-mEos4b-gephyrin^{wt} (N-terminally tagged rat gephyrin, GenBank X66366, splice variant P1) and its PKA-insensitive variant FU-mEos4b-gephyrin^{PKA-} (S294A/S295A/S303A/S305A/S319A) were derived from an earlier construct (Patrizio et al., 2017). The putative PKA target sites were selected based on *in vivo* phosphorylation sites of gephyrin in the PhosphoSitePlus database (www.phosphosite.org; Hornbeck et al., 2015). Another gephyrin construct (mRFP-gephyrin; Calamai et al., 2009) was used for co-transfection together with N- and C-terminal fusion constructs of mEos4b with the cds of mouse EPAC2 (RapGef4, Source BioScience clone IRCLp5011D1135D, IMAGE clone ID IMAGE:40141811) in the FUGW vector.

Lentivirus production

Lentiviruses were produced as described previously (Grünewald et al., 2018). Briefly, HEK-293 cells were co-transfected with replicon DNA together with the two packaging plasmids pCMVR8.74 and pMD2.G (Addgene, plasmids #22036 and #12259) using lipofectamine 2000 (Thermo Fisher Scientific). Cells were kept in Neurobasal medium containing GlutaMAX and B27 at 32°C / 5% CO_2 for 24 h, at which time the medium was replaced. The lentivirus-containing medium was collected at 48-55 h after transfection, filtered with a pore size of 0.45 μm, and stored at -80°C.

Primary neuron cultures

Animals were treated in accordance with the guidelines of the French Ministry of Agriculture and the Direction Départementale des Services Vétérinaires de Paris (Ecole Normale Supérieure, Animalerie des Rogeurs, license B 75-05-20). Dissociated cultures of spinal cord neurons were prepared from Sprague Dawley rat embryos at developmental stage E14 and from mouse embryos at E13 as described previously (Specht et al., 2013), using heterozygous knock-in animals expressing mRFP-tagged gephyrin (Machado et al., 2011) in the C57BL/6J genomic background. Neurons were plated at a density of 1.6 x 10^4/cm^2 on 18 mm coverslips in Neurobasal medium containing GlutaMAX (Thermo Fisher), B27 (Thermo Fisher) and antibiotics. At day *in vitro* (DIV) 7 half of the medium was replaced with BrainPhys neuronal medium (STEMCELL Technologies), and thereafter twice a week. Spinal cord neurons were infected at DIV1-7 if required, and used for experiments at DIV14-20.

Organotypic slice cultures were prepared as previously described (Cantaut-Belarif et al., 2017). Spinal cords from mRFP-gephyrin KI animals at postnatal day P3-P7 were sliced using a McIllwain tissue chopper. Slices of 200 μm thickness were placed on Millicell CM inserts (Millipore) and cultured with MEM medium supplemented with 20% horse serum, 5% HBSS, GlutaMAX, 8 mM D-glucose, 20 mM HEPES and antibiotics. The medium was changed every 3 days and slice cultures were used for experiments up to DIV21.

Pharmacology for immunocytochemistry

Forskolin (Tocris) was dissolved in ethanol at a concentration of 10 mM, and used at a final concentration of 20 μM in culture medium for 30 min unless otherwise stated. In most experiments with forskolin, we used 0.2% ethanol as control condition (vehicle) except for the data shown in figures 2AB, 4AB, S1DE, S4 and S5. In these experiments, no ethanol was added in the control. The PKA antagonist H-89 (Sigma) was used at a final concentration of 2.5 μM. For the activation of EPAC, the cAMP analog 007-AM (8-(4-chloro-phenylthio)-2'-O-methyladenosine-3',5'-cyclic monophosphate acetoxymethyl ester; Tocris) was dissolved in DMSO at 5 mM and applied at a final concentration of 3 μM; the appropriate concentration of DMSO (0.06%) was added in the control condition of the experiments with 007. For immunocytochemistry, PP1/PP2a were blocked with 40 nM okadaic acid for 15 min prior to the treatment with Forskolin and H-89 for an additional 30 min (in the presence of okadaic acid). For details about the application of forskolin and 007-AM in the QD-SPT recordings see below.

Western blotting

Dissociated spinal cord neurons cultured in 6 well plates and infected with mEos4b-gephyrin lentivirus were treated at DIV14 with 20 μM forskolin or vehicle for 30 min (2 wells per condition), and collected on ice with buffer containing 50 mM Tris pH 7.5, 150 mM NaCl, 1% Nonidet P40 and 0.25% SDS, as well as protease inhibitors (complete EDTA-free, Roche) and phosphatase inhibitors (1 mM sodium orthovanadate, 1 mM sodium fluoride, 1 mM sodium molybdate, 4 mM sodium tartrate, 100 nM fenvalerate and 250 nM okadaic acid). Samples were loaded in reducing sample buffer and separated by SDS-PAGE, blotted onto PVDF membranes (Millipore), and labelled with mouse monoclonal anti-gephyrin antibody mAb7a (147 011, Synaptic Systems; Kuhse et al., 2012) and HRP-coupled secondary antibody. Antigens were detected by chemiluminescence and quantified with ImageJ. Membranes were stripped in buffer containing β-mercaptoethanol and SDS at 50ºC for 30 min and then re-labelled with anti-gephyrin antibody 3B11 (Synaptic Systems 147 111; Smolinsky et al., 2008).

For quantification, we analysed two sets of samples for each experiments: non-infected neurons and infected neurons, with or without forskolin treatment. The bands corresponding to endogenous gephyrin and recombinant mEos4b-gephyrin were quantified (i.e. 3 pairs of bands for each membrane). The experiment was repeated three times and the statistical analysis was done on the pooled data (i.e. n = 3 x 3 = 9 data pairs).

Immunolabelling

Immunolabelling was done as described by Patrizio et al. (2017). Fixed neurons were permeabilised in PBS with 0.1% Triton X100, blocked in PBS containing 2.5% BSA, and labelled with primary antibodies (rabbit anti-GlyRα1, custom made; mouse anti-gephyrin mAb7a, Synaptic Systems 147 011; rat anti-gephyrin mAb7a, Synaptic Systems 147 208; mouse anti-gephyrin 3B11, Synaptic Systems 147 111; mouse anti-GABA$_A$Rβ3, clone N87/25, NeuroMab 75-149; rabbit anti-Epac1, Abcam ab21236; rabbit anti-Epac2, Abcam ab21238). Primary antibodies were generally applied for 1 hour at a dilution of 1:500 with the exception of the EPAC antibodies (used at 1:200, 5 μg/ml), followed by secondary goat antibodies (Alexa Fluor 488 conjugated anti-mouse IgG, Cy3 anti-rabbit IgG, Alexa Fluor 647 anti-rat, Alexa Fluor 647 anti-mouse).

Live surface labeling of GlyRα1 was done as follows. Neurons were treated with 20 μM forskolin or vehicle (ethanol) for 15 min in culture medium at 37°C. Then, rabbit anti-GlyRα1 antibody was added at a 1:100 dilution for another 15 min. After fixation and blocking, GlyRs were labelled using secondary Alexa Fluor 488 conjugated anti-rabbit IgG.

Fluorescence image acquisition and analysis

Images of dissociated cultured neurons were acquired on an inverted Nikon Eclipse Ti microscope with a 100x oil-immersion objective (NA 1.49), using an Andor iXon EMCCD camera (16-bit, image pixel size: 160 nm, or 107 nm with an additional 1.5x lens in the emission path) and NIS-Elements software (Nikon). Specific emission filters were chosen for the detection of the different fluorophores: 525/30 for Alexa Fluor 488, unconverted Dendra2 and mEos4b, 607/36 for mRFP and Cy3, and 684/24 for Alexa Fluor 647. Confocal imaging of organotypic slices was done on an SP8 confocal microscope (Leica Microsystems). Nine consecutive single plane images were taken from the dorsal edge of the spinal cord slice towards the ventral region.

Images were always acquired with the same excitation intensity and exposure time in each channel for a given experiment to ensure comparability between experimental conditions. Quantitation was performed using a lab-made programme (ImAnalysis; Hennekinne et al., 2013) in Matlab (MathWorks). Binary masks of synaptic clusters of at least 3 pixels were created by image segmentation with multidimensional image analysis (MIA, Racine et al., 2007; or Spot Detector in Icy, de Chaumont et al., 2012, http://icy.bioimageanalysis.org/). Generally, the gephyrin image was used to generate the binary masks (mRFP-gephyrin in Fig. 2C-E, mEos4b in Fig. 4A-C and S1DE, 3B11 in Fig. 4G), with the exception of the data in figures 1, 2AB, 4E, S4 and S5, where the GlyR images were used to make the mask. For each cluster, the integrated fluorescence intensity was measured in each channel. In some experiments, data were background corrected using readings of diffuse fluorescence intensity in dendrites (Fig. 2AB, 4AB, S1, S4, S5).

Single molecule localisation microscopy (SMLM)

SMLM imaging was done as described elsewhere (Izeddin et al., 2011). Neurons expressing mEos4b-gephyrin were fixed and imaged in PBS in an open chamber. PALM movies of 10000 frames were recorded at 20 Hz with inclined 561 nm laser illumination (output power 40% of 500 mW, emission filter 607/36). mEos4b was photoconverted by 0.5 ms pulsed 405 nm laser illumination with a fixed intensity profile (output power during frames 1-1000 at 2%, 1000-5000 3%, 5000-10000 5% of a 120 mW laser). The focal plane was maintained using a Nikon perfect focus system. For STORM imaging, cultures were immunolabelled with mAb7a and Alexa Fluor 647 antibodies and imaged in STORM buffer composed of 10% glucose, 50 µM β-mercaptoethylamine, 0.5 mg/ml glucose oxidase, and 54 µg/ml catalase in PBS (pH 7.4). Movies of 10000 frames were acquired at 20 Hz with inclined 633 nm laser illumination (output power 80% of 800 mW, emission filter 684/24) and low intensity pulsed photoactivation at 405 nm (output power during frames 1-1000 at 0%, 1000-5000 20%, 5000-10000 50%).

Single fluorophores where detected by Gaussian fitting. The resulting pointillist images were corrected for drifts in the x/y plane using several dense clusters of detections in the images themselves as reference. Quantification of clusters of gephyrin in the pointillist images was done using a lab-made software in Matlab (CountMol; Patrizio et al., 2017). Synaptic clusters were detected by setting a lower threshold for cluster size (minimum length PALM: 100 nm; STORM: 100 nm), as well as the minimum number of detections (PALM: 200 detections; STORM: 50 detections).

Single-particle tracking (SPT)

The diffusion of Dendra2-tagged receptors expressed in spinal cord neurons was analysed by single-particle tracking (SPT) using quantum dots (QDs) as described before (Bannai et al., 2006; Patrizio et al., 2017). Cells were labelled with rabbit Dendra2 antibody (Antibodies-online ABIN361314) and anti-rabbit F(ab')$_2$ coupled QDs emitting at 605 nm, and imaged for up to 30 min in MEM based imaging buffer supplemented with 20 mM HEPES, 2 mM glutamine, 1 mM sodium pyruvate, 2% FBS and 33 mM glucose at 37°C. In the experiments shown in Fig. 6A, B, forskolin, 007-AM and vehicle (0.2% ethanol) were present during QD labelling and recording. For

the data in Fig. 6C, D, forskolin was pre-applied for 30 min, but absent during imaging. Synapses were stained with 1 μM FM4-64 dye applied in imaging buffer containing 40 mM KCl for 30 sec. Synaptic masks were created from these images using Spot Detector in Icy. QD trajectories (500 frames at 13 Hz) were analysed using homemade software in Matlab (Mathworks). Diffusion coefficients of QD-receptors were calculated by fitting of the first 5 points of the mean squared displacement (MSD) plot against time.

Statistical analysis

Immunocytochemical data were analysed with one-way ANOVA and Tukey's test for post hoc analysis, the Kruskal-Wallis (KW) test with Dunn's test for post hoc analysis, or with Welch's t-test. Western blot data were compared using a paired t-test that paired the corresponding conditions in each experiment. QD diffusion data were statistically compared using KW test and Dunn's post hoc test. SMLM data were analysed with Mann-Whitney's U-test (MW). A summary of the statistical information is provided in Table S1 (including tests, sample size, probabilities); Table S2 is a compilation of all the mean values and quartiles displayed in the figures.

References

Bannai, H., Levi, S., Schweizer, C., Dahan, M., and Triller, A. (2006). Imaging the lateral diffusion of membrane molecules with quantum dots. Nat Protoc *1*, 2628-2634.

Calamai, M., Specht, C.G., Heller, J., Alcor, D., Machado, P., Vannier, C., and Triller, A. (2009). Gephyrin oligomerization controls GlyR mobility and synaptic clustering. J Neurosci *29*, 7639-7648.

Cantaut-Belarif, Y., Antri, M., Pizzarelli, R., Colasse, S., Vaccari, I., Soares, S., Renner, M., Dallel, R., Triller, A., and Bessis, A. (2017). Microglia control the glycinergic but not the GABAergic synapses via prostaglandin E2 in the spinal cord. J Cell Biol *216*, 2979-2989.

de Chaumont, F., Dallongeville, S., Chenouard, *et al.* (2012). Icy: an open bioimage informatics platform for extended reproducible research. Nat Methods *9*, 690-696.

Grünewald, N., Jan, A., Salvatico, C., Kress, V., Renner, M., Triller, A., Specht, C.G., and Schwarz, G. (2018). Sequences flanking the gephyrin-binding site of GlyRbeta tune receptor stabilization at synapses. eNeuro *5*.

Hennekinne, L., Colasse, S., Triller, A., and Renner, M. (2013). Differential control of thrombospondin over synaptic glycine and AMPA receptors in spinal cord neurons. J Neurosci *33*, 11432-11439.

Hornbeck, P.V., Zhang, B., Murray, B., Kornhauser, J.M., Latham, V., and Skrzypek, E. (2015). PhosphoSitePlus, 2014: mutations, PTMs and recalibrations. Nucleic Acids Res *43*, D512-520.

Izeddin, I., Specht, C.G., Lelek, M., Darzacq, X., Triller, A., Zimmer, C., and Dahan, M. (2011). Super-resolution dynamic imaging of dendritic spines using a low-affinity photoconvertible actin probe. PLoS One *6*, e15611.

Kuhse, J., Kalbouneh, H., Schlicksupp, A., Mukusch, S., Nawrotzki, R., and Kirsch, J. (2012). Phosphorylation of gephyrin in hippocampal neurons by cyclin-dependent kinase CDK5 at Ser-270 is dependent on collybistin. J Biol Chem *287*, 30952-30966.

Lois, C., Hong, E.J., Pease, S., Brown, E.J., and Baltimore, D. (2002). Germline transmission and tissue-specific expression of transgenes delivered by lentiviral vectors. Science *295*, 868-872.

Machado, P., Rostaing, P., Guigonis, J.M., Renner, M., Dumoulin, A., Samson, M., Vannier, C., and Triller, A. (2011). Heat shock cognate protein 70 regulates gephyrin clustering. J Neurosci *31*, 3-14.

Nikolic, Z., Laube, B., Weber, R.G., Lichter, P., Kioschis, P., Poustka, A., Mulhardt, C., and Becker, C.M. (1998). The human glycine receptor subunit alpha3. Glra3 gene structure, chromosomal localization, and functional characterization of alternative transcripts. J Biol Chem *273*, 19708-19714.

Patrizio, A., Renner, M., Pizzarelli, R., Triller, A., and Specht, C.G. (2017). Alpha subunit-dependent glycine receptor clustering and regulation of synaptic receptor numbers. Sci Rep *7*, 10899.

Racine, V., Sachse, M., Salamero, J., Fraisier, V., Trubuil, A., and Sibarita, J.B. (2007). Visualization and quantification of vesicle trafficking on a three-dimensional cytoskeleton network in living cells. J Microsc *225*, 214-228.

Smolinsky, B., Eichler, S.A., Buchmeier, S., Meier, J.C., and Schwarz, G. (2008). Splice-specific functions of gephyrin in molybdenum cofactor biosynthesis. J Biol Chem *283*, 17370-17379.

Specht, C.G., Izeddin, I., Rodriguez, P.C., El Beheiry, M., Rostaing, P., Darzacq, X., Dahan, M., and Triller, A. (2013). Quantitative nanoscopy of inhibitory synapses: counting gephyrin molecules and receptor binding sites. Neuron *79*, 308-321.
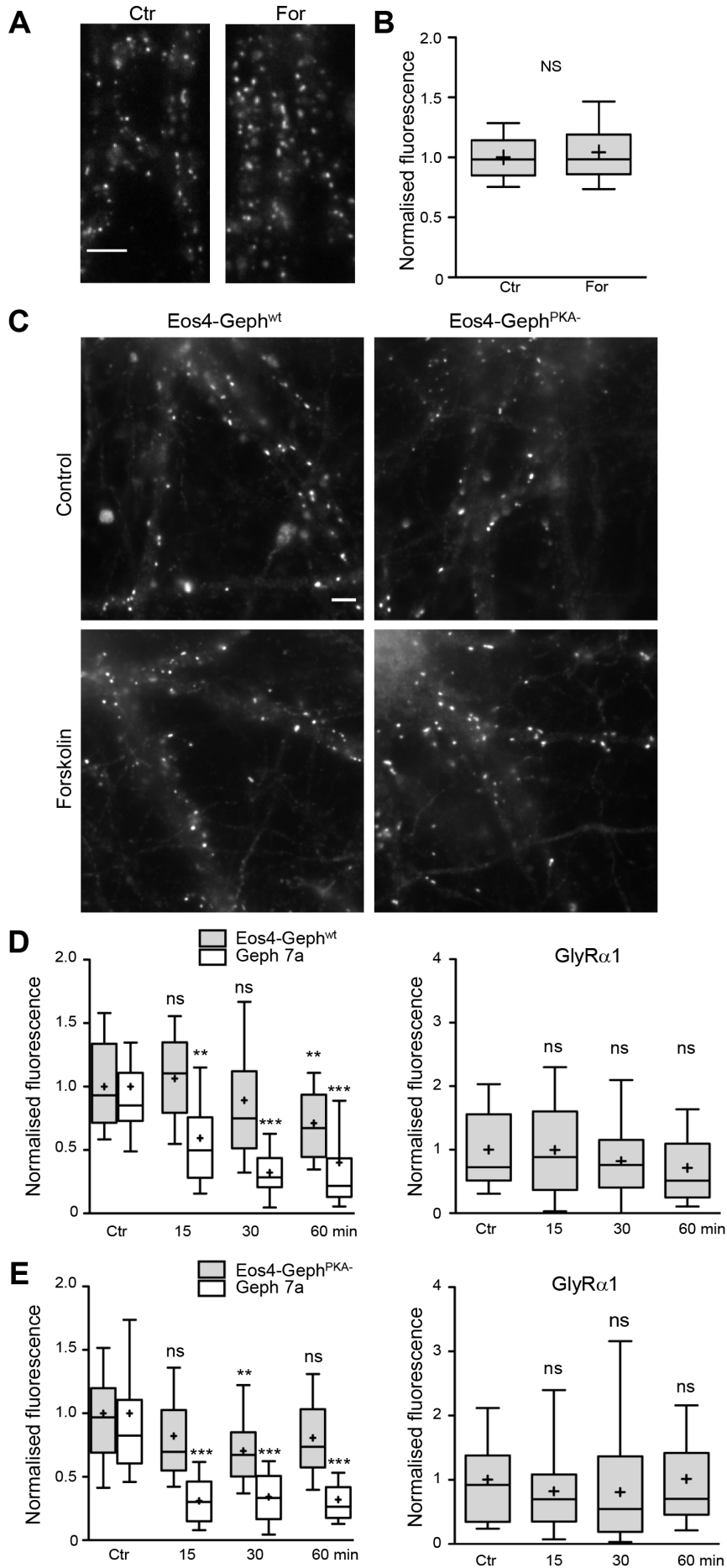
Figure S1. Effect of forskolin on GlyRα1 and gephyrin (related to Fig. 1).
(A) Immunocytochemistry of surface labelled GlyRα1 treated with or without forskolin. Scale: 5 μm. **(B)** Quantification of fluorescence intensity of surface GlyRα1 clusters (n_{Ctr} = 80, n_{For} = 80 cells from 2 experiments; p = 0.27, t-test). **(C)** Overview images of Eos4-Geph^{wt} and Eos4-Geph^{PKA-} expressing neurons with or without forskolin treatment, showing proximal dendrites crossing the whole image. Scale: 5 μm. **(D)** Eos4-Geph^{wt} and **(E)** Eos4-Geph^{PKA-} expressing neurons were treated with forskolin for 15, 30 or 60 min, or without forskolin (Ctr), fixed and labelled with anti-GlyRα1 and mAb7a antibodies. Both, neurons expressing Eos4-Geph^{wt} and Eos4-Geph^{PKA-} showed a significant reduction of gephyrin phosphorylation (mAb7a) in response to forskolin, whereas total mEos4-gephyrin levels and GlyRα1 labelling remained relatively stable. Data were normalised to the control condition in each channel for each construct and each experiment. Note that the left panels in (D, E) are the same data as those used to calculate the mAb7a/Eos4 ratios in Fig. 4B. Data are represented as 10%, 25%, 50%, 75% and 90% percentiles; the mean is indicated as a cross; **p < 0.01, ***p < 0.001, ANOVA.
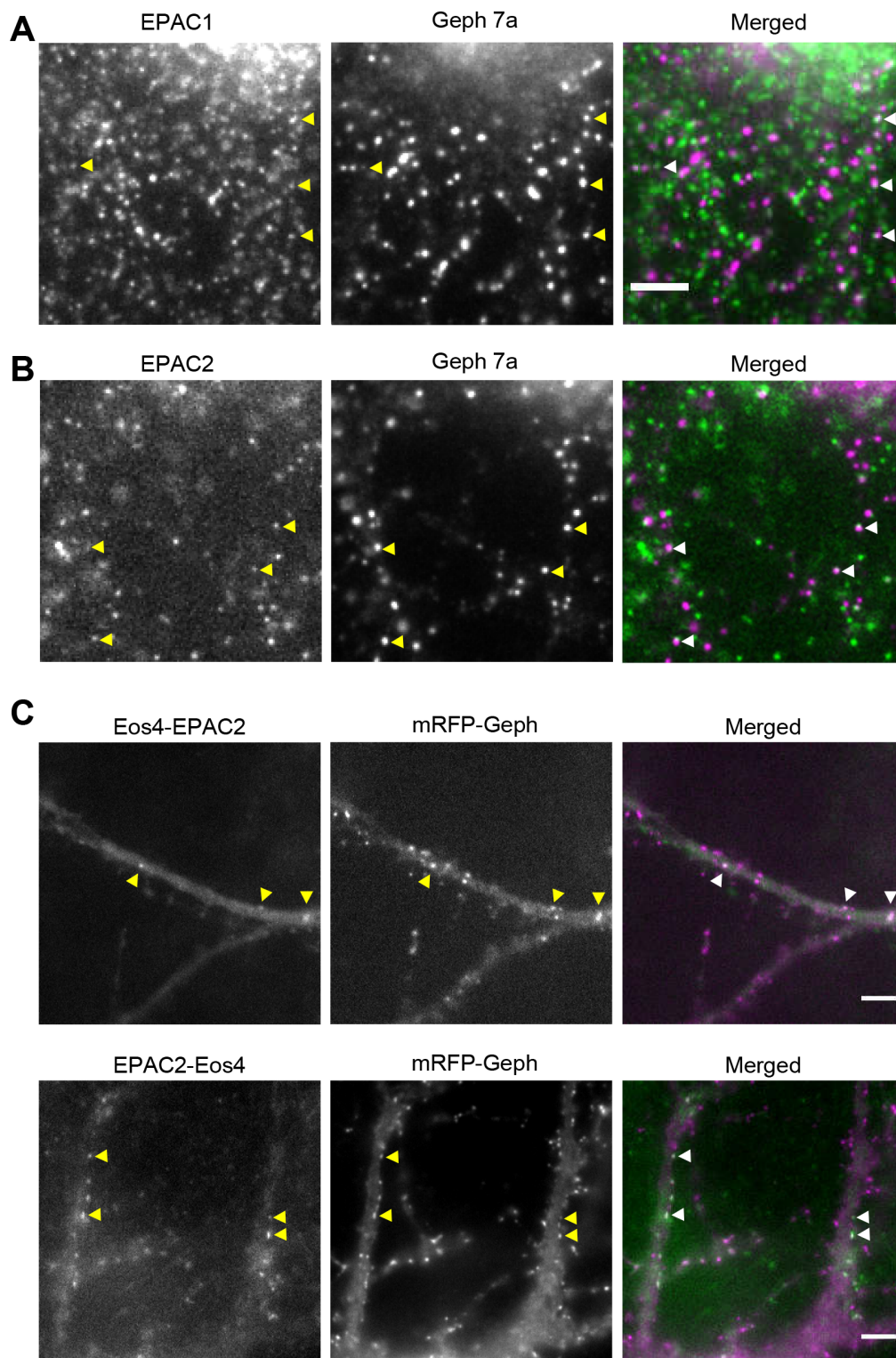
Figure S2. EPAC is present at inhibitory synapses in spinal cord neurons (related to Fig. 4).
Cultured rat spinal cord neurons were immunolabelled with antibodies against EPAC1 **(A)** and EPAC2 **(B)**, as well as with the gephyrin antibody mAb7a. The partial co-localisation of the EPAC proteins (shown in green in the merged images) and the inhibitory synaptic gephyrin scaffold (red) is indicated by arrowheads. **(C)** Spinal cord neurons co-transfected with mRFP-gephyrin (magenta) and N- or C-terminally tagged EPAC2 (constructs FU-mEos4b-EPAC2 and FU-EPAC2-mEos4b, green). EPAC2 co-localises with a sub-population of mRFP-gephyrin clusters (arrowheads) at inhibitory synapses. Scale: 5 µm.
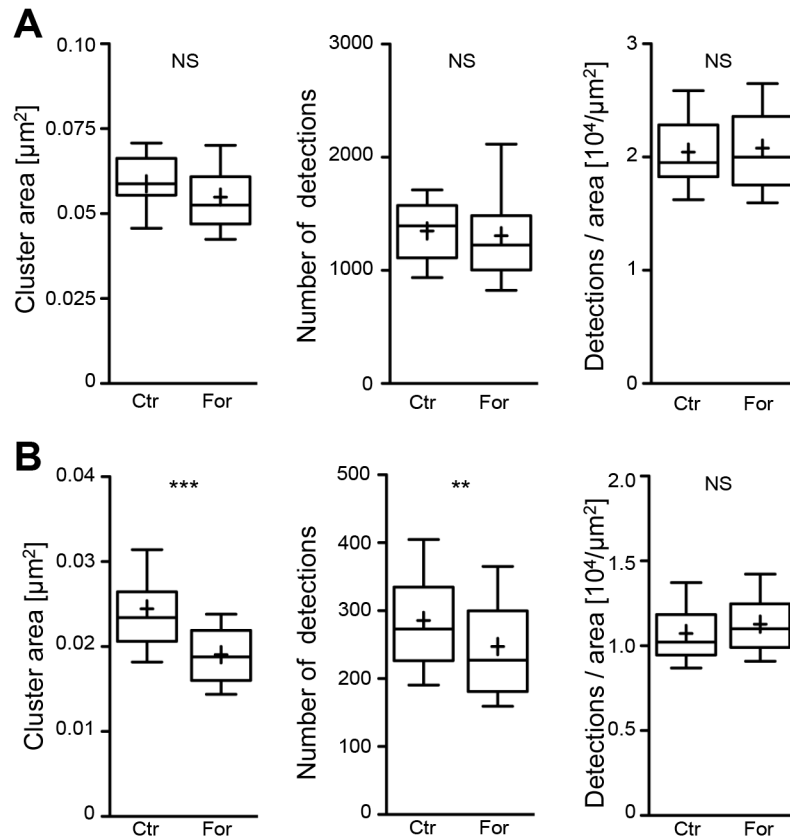
Figure S3. Cell by cell analysis of SMLM data of synaptic gephyrin clusters (related to Fig. 5).
(A) Quantification of synaptic cluster areas, detection numbers, and detection densities by PALM imaging with mEos4b-gephyrin (n_{Ctr} = 32, for n_{For} = 32 cells from 3 independent experiments; area p = 0.65, detections p = 0.14, detection/area p = 0.73, t-test). **(B)** The quantification of cluster area and number of mAb7a (Alexa 647) detections in dSTORM images shows a correlated decrease in forskolin treated neurons compared to control (n_{Ctr} = 70, for n_{For} = 66 from 3 independent experiments; area ***p < 0.0001, detections **p < 0.01, detection/area p = 0.09, t-test). Cell by cell analysis did not reveal any significant differences in the detection densities of total (Eos4, **A**) or pS270-gephyrin (mAb7a, **B**), in contrast to the synapse by synapse analysis of the same dataset (see Fig. 5).
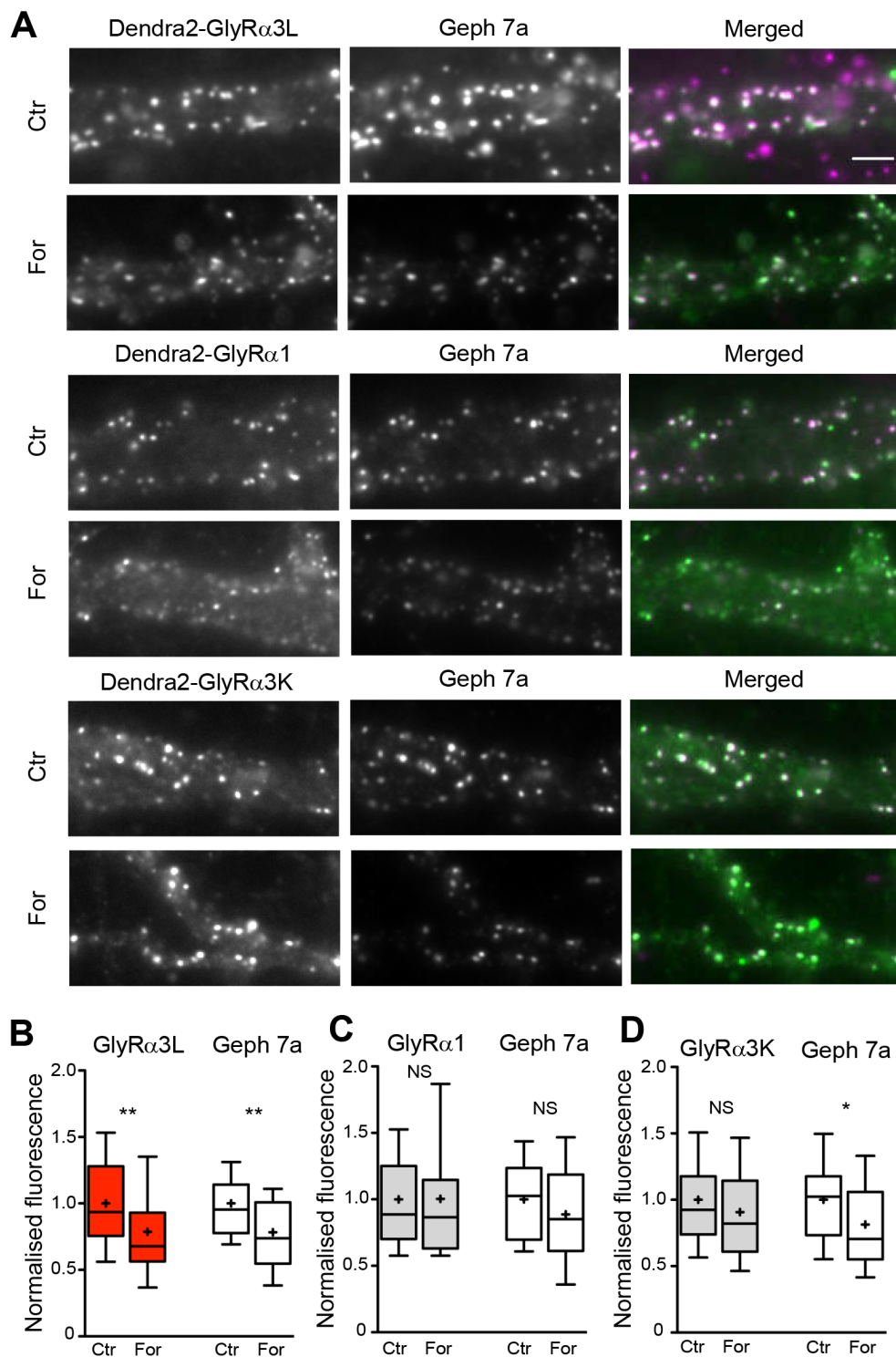
Figure S4. Forskolin specifically alters GlyRα3L levels at synapses (related to Fig. 6).
(A) Lentivirus-infected rat spinal cord neurons expressing Dendra2-GlyRα1, α3K, or α3L (green in merged image) were treated with or without forskolin, fixed, and labelled with mAb7a antibody (magenta in merged image). Scale: 5 µm. **(B)** Dendra2-GlyRα3L fluorescence levels at synapses were decreased by $22 \pm 5\%$ following 30 min of treatment with forskolin ($n_{Ctr} = 70$, $n_{For} = 61$ cells from 3 experiments). **(C)** Dendra2-GlyRα1 fluorescence at synapses was not affected by forskolin ($n_{Ctr} = 53$, $n_{For} = 32$). **(D)** Forskolin did not alter the levels of synaptic Dendra2-GlyRα3K ($n_{Ctr} = 68$, $n_{For} = 69$). Gephyrin labelling with the phospho-specific antibody mAb7a at Dendra2 puncta was consistently reduced in all experiments (B-D). Data are represented as 10%, 25%, 50%, 75% and 90% percentiles and the mean (as cross); *$p < 0.05$, **$p < 0.01$, ANOVA.
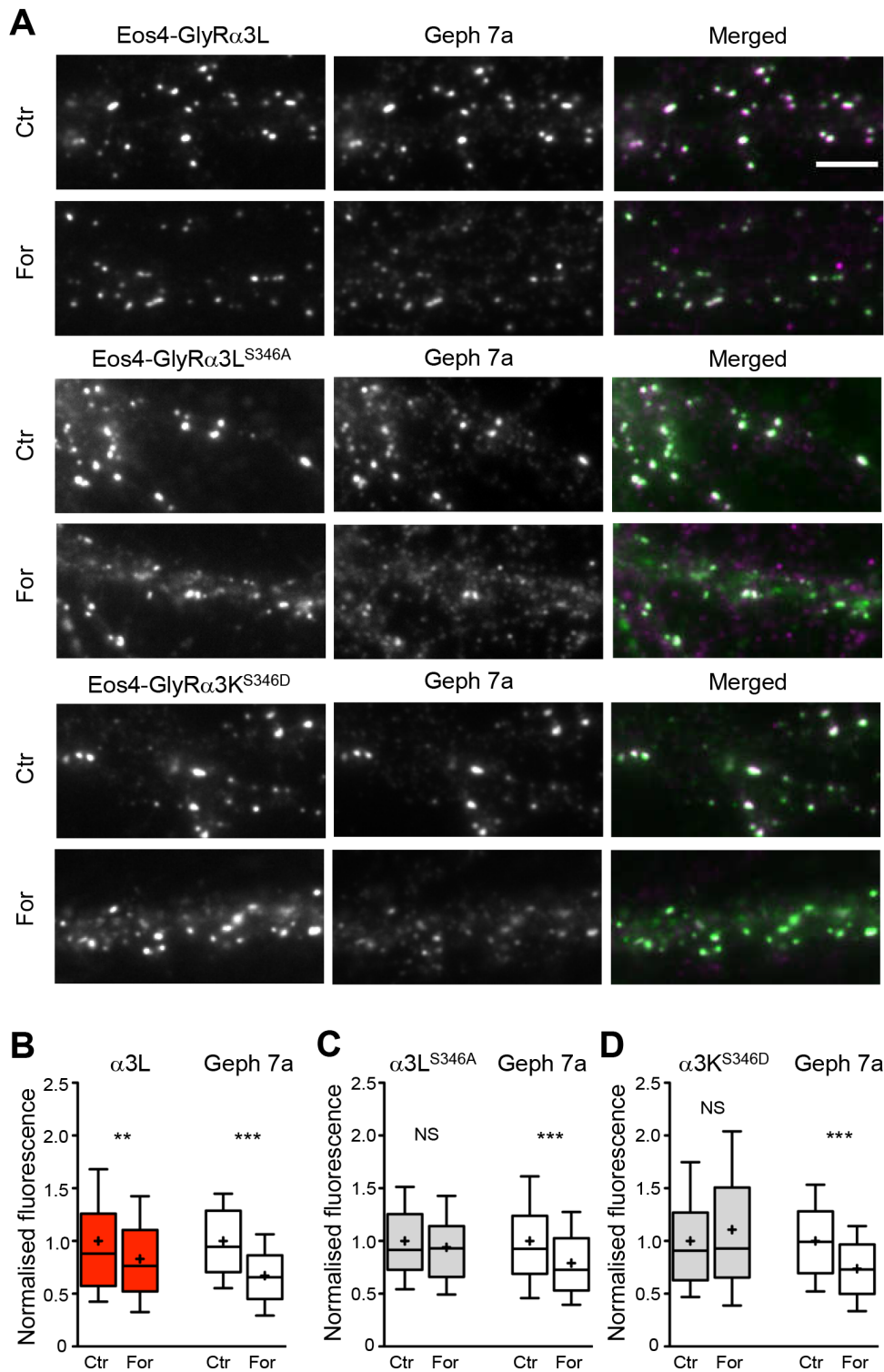
Figure S5. GlyRα3L clustering is regulated by S346 phosphorylation (related to Fig. 6).
(A) Lentivirus-infected rat spinal cord neurons expressing wildtype Eos4-GlyRα3L or the phosphorylation mutants Eos4-GlyRα3L^{S346A} or Eos4-GlyRα3L^{S346D} (green) were treated with or without forskolin, fixed, and labelled with mAb7a antibody (magenta). Scale: 5 μm. **(B-D)** Gephyrin labelling with the phospho-specific antibody mAb7a was consistently reduced at synapses by 30 min of treatment with forskolin, as was Eos4-GlyRα3L fluorescence (**B**, n_{Ctr} = 146, n_{For} = 159 cells from 3 experiments). In contrast, Eos4-GlyRα3L^{S346A} (**C**, n_{Ctr} = 159, n_{For} = 146) and Eos4-GlyRα3L^{S346D} levels (**D**, n_{Ctr} = 164, n_{For} = 141) at synapses were not affected by forskolin treatment. Data are shown as percentiles of the population (10%, 25%, 50%, 75%, 90%) and the mean (cross); **$p < 0.01$, ***$p < 0.001$, ANOVA.

Table S1. Statistical evaluation of the data including applied tests, sample size, and p-values (related to Figures 1-6).

Figure Number	Used Statistics	Type of sample	Type of analysis	Sample number (n)	P value
Fig. 1B	1 way anova with Tukey's Multiple comparison test as post hoc test	Mean intensity of each cluster in a cell	Cell by cell	$n_{Ctr} = 86$, $n_{For} = 79$	P<0.0001
Fig. 1C	1 way anova with Tukey's Multiple comparison test as post hoc test	Ratio of receptor / gephyrin in each cluster	cluster by cluster	$n_{Ctr} = 14218$, $n_{For} = 12334$	P<0.0001
Fig. 2B	1 way anova with Tukey's Multiple comparison test as post hoc test	Mean intensity of each cluster in a cell	Cell by cell	GlyRa1: $n_{Ctr} = 149$, $n_{For} = 144$; mAb7a: $n_{Ctr} = 60$, $n_{For} = 56$; 3B11: $n_{Ctr} = 89$, $n_{For} = 88$	P<0.0001
Fig. 2D	1 way anova with Tukey's Multiple comparison test as post hoc test	Mean intensity of each cluster in a cell	Cell by cell	$n_{Ctr} = 39$, $n_{For} = 40$	P=0.5651
Fig. 2E Control vs forskolin	Welch's t test	Mean intensity of each cluster in an image	image by image	$n_{Ctr} = 44$, $n_{For} = 57$	P<0.0001
Fig. 2E comparison of different timepoint	1 way anova with Tukey's Multiple comparison test as post hoc test	Mean intensity of each cluster in an image	image by image	$n_{Ctr2-3} = 14$, $n_{Ctr4-5} = 14$, $n_{Ctr6-7} = 10$, $n_{Ctr8-9} = 6$, $n_{For2-3} = 16$, $n_{For4-5} = 16$, $n_{For6-7} = 13$, $n_{For8-9} = 12$,	Ctr P=0.1255 , For P=0.0721
Fig. 3B	Paired t test	Mean intensity of each band in each condition	Condition per condition	$n_{Ctr} = 9$, $n_{For} = 9$; 3 experiment, each contains 3 bands (endogenous, Eos4-geph, endogenous in Eos4-geph infected)	P<0.0001
Fig. 4B	Kruskal-Wallis test with Dunn's test as post hoc test	Mean intensity of each cluster in a cell	Cell by cell	$n_{Eos4-GephWTCtr} = 44$, $n_{Eos4-GephWT15} = 44$, $n_{Eos4-GephWT30} = 44$, $n_{Eos4-GephWT60} = 44$, $n_{Eos4-GephPKA-Ctr} = 42$, $n_{Eos4-GephPKA-15} = 43$, $n_{Eos4-GephPKA-30} = 44$, $n_{Eos4-GephPKA-60} = 45$	P<0.0001
Fig. 4C	1 way anova with Tukey's Multiple comparison test as post hoc test	Mean intensity of each cluster in a cell	Cell by cell	$n_{Ctr} = 60$, $n_{For} = 60$, $n_{For/H-89} = 60$	P<0.0001
Fig. 4E	1 way anova with Tukey's Multiple comparison test as post hoc test	Mean intensity of each cluster in a cell	Cell by cell	$n_{Ctr} = 90$, $n_{007} = 83$	P<0.0001
Fig. 4G	1 way anova with Tukey's Multiple comparison test as post hoc test	Mean intensity of each cluster in a cell	Cell by cell	$n_{Ctr} = 86$, $n_{For + Oka} = 84$	P<0.0001
Fig. 5B	Mann Whitney U test	Each value for each cluster	Cluster by cluster	$n_{Ctr} = 1237$, $n_{For} = 894$	Area P=0.1992; Detection P=0.8702; Detection/area P=0.0289
Fig. 5D	Mann Whitney U test	Each value for each cluster	Cluster by cluster	$n_{Ctr} = 8162$, $n_{For} = 7010$	Area P<0.0001; Detection P=0.0001; Detection/area P=0.0001
Fig. 6B	Kruskal-Wallis test with Dunn's test as post hoc test	D per each trajectory	Trajectory by trajectory	$n_{Ctr} = 730$, $n_{For} = 318$, $n_{007} = 384$	P<0.0001
Fig. 6C	Mann Whitney U test	D per each trajectory	Trajectory by trajectory	$n_{Ctr} = 1315$, $n_{For} = 1074$	P=0.0477
Fig. 6D	Mann Whitney U test	D per each trajectory	Trajectory by trajectory	a3L $n_{Ctr} = 1661$, $n_{For} = 1546$; a3K $n_{Ctr} = 1315$, $n_{For} = 1074$	a3L P<0.0001; a3K P=0.1304
Fig. S1B	Welch's t-test	Mean intensity of each cluster in a cell	Cell by cell	$n_{Ctr} = 80$, $n_{For} = 80$	P=0.2744
Fig. S1D Eos4 vs 7a	Kruskal-Wallis test with Dunn's test as post hoc test	Mean intensity of each cluster in a cell	Cell by cell	$n_{Eos4-GephWTCtr} = 44$, $n_{Eos4-GephWT15} = 44$, $n_{Eos4-GephWT30} = 44$, $n_{Eos4-GephWT60} = 44$	Eos P<0.0001, 7a P<0.0001
Fig. S1D GlyRa1	Kruskal-Wallis test	Mean intensity of each cluster in a cell	Cell by cell	$n_{Eos4-GephWTCtr} = 44$, $n_{Eos4-GephWT15} = 44$, $n_{Eos4-GephWT30} = 44$, $n_{Eos4-GephWT60} = 44$	P=0.0729
Fig. S1E Eos4 vs 7a	Kruskal-Wallis test with Dunn's test as post hoc test	Mean intensity of each cluster in a cell	Cell by cell	$n_{Eos4-GephPKA-Ctr} = 42$, $n_{Eos4-GephPKA-15} = 43$, $n_{Eos4-GephPKA-30} = 44$, $n_{Eos4-GephPKA-60} = 45$	Eos P=0.0085, 7a P<0.0001
Fig. S1E GlyRa1	Kruskal-Wallis test	Mean intensity of each cluster in a cell	Cell by cell	$n_{Eos4-GephPKA-Ctr} = 42$, $n_{Eos4-GephPKA-15} = 43$, $n_{Eos4-GephPKA-30} = 44$, $n_{Eos4-GephPKA-60} = 45$	P=0.2454
Fig. S3A	Welch's t-test	Mean value of each cluster in a image	Image by image	$n_{Ctr} = 32$, $n_{For} = 32$	Area P=0.6528; Detection P=0.1433; Detection/area P=0.7279
Fig. S3B	Welch's t-test	Mean value of each cluster in a image	Image by image	$n_{Ctr} = 70$, $n_{For} = 66$	Area P<0.0001; Detection P=0.0094; Detection/area P=0.0908
Fig. S4B	1 way anova with Tukey's Multiple comparison test as post hoc test	Mean intensity of each cluster in a cell	Cell by cell	$n_{Ctr} = 69$, $n_{For} = 60$	P<0.0001
Fig. S4C	1 way anova	Mean intensity of each cluster in a cell	Cell by cell	$n_{Ctr} = 51$, $n_{For} = 31$	P=0.6265
Fig. S4D	1 way anova with Tukey's Multiple comparison test as post hoc test	Mean intensity of each cluster in a cell	Cell by cell	$n_{Ctr} = 68$, $n_{For} = 69$	P=0.0121
Fig. S5B	1 way anova with Tukey's Multiple comparison test as post hoc test	Mean intensity of each cluster in a cell	Cell by cell	$n_{Ctr} = 146$, $n_{For} = 159$	P<0.0001
Fig. S5C	1 way anova with Tukey's Multiple comparison test as post hoc test	Mean intensity of each cluster in a cell	Cell by cell	$n_{Ctr} = 159$, $n_{For} = 146$	P<0.0001
Fig. S5D	1 way anova with Tukey's Multiple comparison test as post hoc test	Mean intensity of each cluster in a cell	Cell by cell	$n_{Ctr} = 164$, $n_{For} = 141$	P<0.0001

Table S2. Compilation of mean values and quartiles of the data in each graph (related to Figures 1-6).

Figure Number	mean	25%	median	75%
Fig. 1B GlyR Ctr	1	0.8419	0.9639	1.179
Fig. 1B GlyR For	0.9347	0.7528	0.8727	1.055
Fig. 1B GABA$_A$R Ctr	1	0.8516	0.9954	1.128
Fig. 1B GABA$_A$R For	0.8023	0.7088	0.8422	0.9403
Fig. 1B Geph 7a Ctr	1	0.8497	0.9512	1.182
Fig. 1B Geph 7a For	0.766	0.6166	0.7416	0.926
Fig. 1C GlyR/ 7a Ctr	1.176	0.8168	0.9931	1.205
Fig. 1C GlyR/ 7a For	1.564	0.9448	1.174	1.833
Fig. 1C GABA$_A$R/ 7a Ctr	1.09	0.8105	0.9997	1.253
Fig. 1C GABA$_A$R/ 7a For	1.178	0.789	1.044	1.431
Fig. 2B GlyR Ctr	1	0.5024	0.8338	1.323
Fig. 2B GlyR For	1.022	0.5111	0.8267	1.429
Fig. 2B Geph 7a Ctr	1	0.646	0.878	1.366
Fig. 2B Geph 7a For	0.5528	0.313	0.4519	0.6843
Fig. 2B Geph 3B11 Ctr	1	0.7992	0.9556	1.162
Fig. 2B Geph 3B11 For	0.9309	0.672	0.8848	1.092
Fig. 2D GlyR Ctr	1	0.7779	0.932	1.149
Fig. 2D GlyR For	1.014	0.6498	0.8532	1.133
Fig. 2D mRFP-Geph KI Ctr	1	0.769	0.9119	1.104
Fig. 2D mRFP-Geph KI For	0.884	0.6617	0.7812	1.077
Fig. 2E Ctr 2-3	0.8981	0.8032	0.8885	1.084
Fig. 2E Ctr 4-5	1.093	0.8971	1.022	1.075
Fig. 2E Ctr 6-7	1.021	0.924	1.063	1.119
Fig. 2E Ctr 8-9	1.123	1.065	1.123	1.187
Fig. 2E For 2-3	0.6681	0.4978	0.7131	0.8416
Fig. 2E For 4-5	0.7668	0.7246	0.8141	0.8588
Fig. 2E For 6-7	0.7985	0.7567	0.8121	0.9348
Fig. 2E For 8-9	0.8208	0.782	0.8463	0.9162
Fig. 3B Ctr	1.01	0.835	0.9861	1.196
Fig. 3B For	0.5517	0.4102	0.5597	0.6281
Fig. 4B Eos-Geph^{wt} Ctr	1	0.5356	0.7982	0.9707
Fig. 4B Eos-Geph^{wt} 15	0.5301	0.2085	0.4522	0.7173
Fig. 4B Eos-Geph^{wt} 30	0.4431	0.1707	0.2994	0.5457
Fig. 4B Eos-Geph^{wt} 60	0.5617	0.179	0.2714	0.5096
Fig. 4B Eos-Geph^{PKA-} Ctr	1	0.6283	0.75	1.057
Fig. 4B Eos-Geph^{PKA-} 15	0.3891	0.2098	0.3515	0.5174
Fig. 4B Eos-Geph^{PKA-} 30	0.4935	0.1953	0.4527	0.5959
Fig. 4B Eos-Geph^{PKA-} 60	0.4454	0.2135	0.3108	0.5395
Fig. 4C Ctr	1	0.7746	0.9813	1.194
Fig. 4C For	0.7968	0.6293	0.7605	0.9153
Fig. 4C For/H-89	0.8213	0.6386	0.766	0.9822
Fig. 4E GlyR Ctr	1	0.8024	0.9548	1.159
Fig. 4E GlyR 007	0.9447	0.7516	0.9273	1.075
Fig. 4E Geph 7a Ctr	1	0.7741	0.9735	1.216
Fig. 4E Geph 7a 007	0.8364	0.5808	0.8334	1.093
Fig. 4E GABA$_A$R Ctr	1	0.7371	0.9739	1.192
Fig. 4E GABA$_A$R 007	0.8368	0.623	0.8002	1.053
Fig. 4G Geph 3B11 For/H-89	1	0.8682	0.9816	1.146
Fig. 4G Geph 3B11 For/H-89/Oka	1.046	0.8617	0.9874	1.243
Fig. 4G Geph 7a For/H-89	1	0.7736	0.991	1.228
Fig. 4G Geph 7a For/H-89/Oka	1.171	0.9326	1.095	1.386
Fig. 5B area Ctr	0.05872	0.0253	0.0412	0.0765
Fig. 5B area For	0.05315	0.025	0.04205	0.0682
Fig. 5B detections Ctr	1316	324.5	657	1847
Fig. 5B detections For	1276	326.8	697	1808
Fig. 5B detections/area Ctr	1.976	1.233	1.666	2.419
Fig. 5B detections/area For	2.09	1.287	1.766	2.53
Fig. 5D area Ctr	0.02468	0.0114	0.01805	0.0302
Fig. 5D area For	0.01986	0.0098	0.0143	0.024
Fig. 5D detections Ctr	298.2	85	158	332
Fig. 5D detections For	259.6	76	127	270
Fig. 5D detections/area Ctr	1.103	0.672	0.8784	1.206
Fig. 5D detections/area For	1.136	0.7037	0.9143	1.245
Fig. 6B GABA$_A$g2 Ctr	0.009697	0.0009782	0.002203	0.004024
Fig. 6B GABA$_A$g2 For	0.01932	0.001768	0.00363	0.005805
Fig. 6B GABA$_A$g2 007	0.01281	0.001559	0.002816	0.005431
Fig. 6C GlyR a1 Ctr	0.0192	0.002985	0.008381	0.02186
Fig. 6C GlyR a1 For	0.01719	0.002333	0.007627	0.01899
Fig. 6C GlyR a3L Ctr	0.01035	0.001262	0.004172	0.01083
Fig. 6C GlyR a3L For	0.01452	0.001976	0.005843	0.0144
Fig. 6C GlyR a3K Ctr	0.0138	0.00214	0.006054	0.01631
Fig. 6C GlyR a3K For	0.01465	0.002427	0.006608	0.01631

Figure Number	mean	25%	median	75%
Fig. S1B Ctr	1	0.8488	0.9829	1.143
Fig. S1B For	1.043	0.86	0.9834	1.191
Fig. S1D Eos-Geph^{wt} Ctr	1	0.7154	0.9307	1.337
Fig. S1D Eos-Geph^{wt} 15	1.065	0.7931	1.105	1.348
Fig. S1D Eos-Geph^{wt} 30	0.8914	0.5138	0.7487	1.121
Fig. S1D Eos-Geph^{wt} 60	0.7714	0.4446	0.6718	0.936
Fig. S1D Geph 7a Ctr (WT)	1	0.7293	0.8516	1.108
Fig. S1D Geph 7a 15 (WT)	0.5939	0.2803	0.4969	0.7579
Fig. S1D Geph 7a 30 (WT)	0.3216	0.208	0.2847	0.4358
Fig. S1D Geph 7a 60 (WT)	0.4013	0.1308	0.2164	0.4347
Fig. S1D GlyRa1 Ctr (WT)	1	0.5136	0.7242	1.558
Fig. S1D GlyRa1 15 (WT)	0.9974	0.3667	0.8857	1.603
Fig. S1D GlyRa1 30 (WT)	0.8195	0.4041	0.76	1.1154
Fig. S1D GlyRa1 60 (WT)	0.7144	0.2483	0.5112	1.094
Fig. S1E Eos-Geph^{PKA-} Ctr	1	0.6906	0.9692	1.199
Fig. S1E Eos-Geph^{PKA-} 15	0.8216	0.5492	0.6972	1.027
Fig. S1E Eos-Geph^{PKA-} 30	0.703	0.5016	0.6724	0.8509
Fig. S1E Eos-Geph^{PKA-} 60	0.806	0.5733	0.7355	1.033
Fig. S1E Geph 7a Ctr (PKA-)	1	0.6045	0.8255	1.106
Fig. S1E Geph 7a 15 (PKA-)	0.3106	0.1491	0.3027	0.4631
Fig. S1E Geph 7a 30 (PKA-)	0.3413	0.1658	0.3339	0.5077
Fig. S1E Geph 7a 60 (PKA-)	0.3205	0.1754	0.2647	0.4188
Fig. S1E GlyRa1 Ctr (PKA-)	1	0.3421	0.9174	1.378
Fig. S1E GlyRa1 15 (PKA-)	0.8233	0.3503	0.6981	1.085
Fig. S1E GlyRa1 30 (PKA-)	0.81	0.1897	0.5456	1.367
Fig. S1E GlyRa1 60 (PKA-)	1.014	0.4568	0.7038	1.419
Fig. S3A area Ctr	0.05881	0.5547	0.0588	0.06628
Fig. S3A area For	0.05486	0.0469	0.05256	0.0609
Fig. S3A detections Ctr	1349	1111	1393	1004
Fig. S3A detections For	1307	1004	1223	1483
Fig. S3A detections/area Ctr	2.043	1.825	1.952	2.284
Fig. S3A detections/area For	2.078	1.753	1.998	2.36
Fig. S3B area Ctr	0.02445	0.0206	0.02341	0.02646
Fig. S3B area For	0.01905	0.01603	0.01877	0.02191
Fig. S3B detections Ctr	285.4	226.4	273	335
Fig. S3B detections For	247.4	181	227.2	299.7
Fig. S3B detections/area Ctr	1.073	0.945	1.022	1.183
Fig. S3B detections/area For	1.128	0.9916	1.1	1.248
Fig. S4B GlyRa3L Ctr	1	0.7556	0.9352	1.279
Fig. S4B GlyRa3L For	0.7865	0.5635	0.6781	0.9304
Fig. S4B Geph 7a Ctr (GlyRa3L)	1	0.7769	0.9543	1.1142
Fig. S4B Geph 7a For (GlyRa3L)	0.7829	0.5475	0.7371	1.008
Fig. S4C GlyRa1 Ctr	1	0.7018	0.887	1.252
Fig. S4C GlyRa1 For	1.004	0.6312	0.8648	1.147
Fig. S4C Geph 7a Ctr (GlyRa1)	1	0.697	1.026	1.236
Fig. S4C Geph 7a For (GlyRa1)	0.8878	0.6122	0.8515	1.187
Fig. S4D GlyRa3K Ctr	1	0.7385	0.9245	1.177
Fig. S4D GlyRa3K For	0.9077	0.6101	0.82	1.144
Fig. S4D Geph 7a Ctr (GlyRa3K)	1	0.7335	1.023	1.176
Fig. S4D Geph 7a For (GlyRa3K)	0.8136	0.5515	0.7047	1.059
Fig. S5B GlyRa3LWT Ctr	1	0.5736	0.8796	1.259
Fig. S5B GlyRa3LWT For	0.8289	0.5212	0.7639	1.104
Fig. S5B Geph 7a Ctr (WT)	1	0.7049	0.9454	1.286
Fig. S5B Geph 7a For (WT)	0.6713	0.4493	0.6567	0.8643
Fig. S5C GlyRa3LS346A Ctr	1	0.7274	0.9158	1.255
Fig. S5C GlyRa3LS346A For	0.9404	0.6599	0.9306	1.141
Fig. S5C Geph 7a Ctr (S346A)	1	0.6889	0.9261	1.238
Fig. S5C Geph 7a For (S346A)	0.7912	0.5303	0.7275	1.026
Fig. S5D GlyRa3LS346D Ctr	1	0.6272	0.9087	1.269
Fig. S5D GlyRa3LS346D For	1.107	0.6542	0.9287	1.506
Fig. S5D Geph 7a Ctr (S346D)	1	0.6945	0.9914	1.281
Fig. S5D Geph 7a For (S346D	0.7374	0.4985	0.7299	0.9673